Exploring a moonlighting function of the large subunit of ribulose-1,5-bisphosphate carboxylase/oxygenase during oxidative stress in *Chlamydomonas reinhardtii*

Kristina Santilli

A Thesis
in
The Department
of
Biology

Presented in Partial Fulfilment of the Requirements
For the Degree of Master of Science (Biology) at
Concordia University
Montréal, Québec, Canada

August 2023

CONCORDIA UNIVERSITY

School of Graduate Studies

This is to certify that the thesis prepared

By: Kristina Santilli

Entitled: Exploring a moonlighting function of the large subunit of ribulose-1,5-bisphosphate carboxylase/oxygenase during oxidative stress in *Chlamydomonas reinhardtii*

and submitted in partial fulfillment of the requirements for the degree of

Master of Science (Biology)

complies with the regulations of the University and meets the accepted standards with respect to originality and quality.

Signed by the final Examining Committee:

_____ Chair
Dr. Aashiq Kachroo

_____ External examiner
Dr. David Kwan

_____ Examiner
Dr. Paul Joyce

_____ Examiner
Dr. Aashiq Kachroo

_____ Thesis Supervisor
Dr. William Zerges

Approved by _____
Chair of Department or Graduate Program Director

August 2023 _____
Dean of Faculty

Abstract

Exploring a moonlighting function of the large subunit of ribulose-1,5-bisphosphate carboxylase/oxygenase during oxidative stress in *Chlamydomonas reinhardtii*

Kristina Santilli

Reactive oxygen species (ROS) are known to oxidize macromolecules, causing them to be non-functional or harmful. When adverse conditions cause the production of ROS to exceed the capacities of antioxidant responses, oxidative stress arises. During stress, RNA granules called chloroplast stress granules form in the chloroplast of *Chlamydomonas reinhardtii*. It is hypothesized that the large subunit of Rubisco, RbcL, has a moonlighting function in oxidative stress tolerance as it localizes to chloroplast stress granules without the small subunit (RbcS), and has an RNA-binding activity that is activated under oxidizing conditions (Uniacke & Zerges, 2008; Yosef *et al.*, 2004). This thesis analyzes multiple RbcL mutants to 1) identify the supramolecular state of RbcL that accumulates during hydrogen peroxide-induced stress tolerance, and 2) characterize whether certain regions of the protein are required for the moonlighting function. My results reveal that it is specifically the RbcL dimer, as well as select mutations in the RNA-binding domain and cysteines, that are involved in this alternate function. I further examine if a correlation exists between enhanced stress tolerance and a Triton X-100 insoluble pool of RbcL. This RbcL subpool was found in four of seven mutants with elevated stress tolerance, partially supporting this hypothesis. I also investigate where this non-Rubisco form of RbcL localizes in the chloroplast. Immunofluorescence microscopy results show RbcL in punctate bodies in mutants that have both excess Triton X-100 insoluble RbcL and elevated stress tolerance. This raises the possibility that RbcL in punctate structures carries out the moonlighting function.

Acknowledgments & Dedications

I would like to take this opportunity to thank an array of individuals who shaped me into a scientist with valuable and diverse skills. Firstly, I wholeheartedly thank my supervisor Dr. William Zerges for his guidance and insightful suggestions throughout my M.Sc. degree. I have grown as a researcher from your mentorship and vast knowledge, and I thank you for giving me this opportunity. Furthermore, a big thank you to my committee members, Dr. Paul Joyce and Dr. Aashiq Kachroo, for their time, helpful comments, and great ideas.

I thank Dr. Katia Wostrikoff for stimulating discussions and providing the supramolecular state mutant strains used in this project.

I thank Dr. Chris Law for all his training, assistance, macro designs and technical advice at the Centre for Microscopy and Cellular Imaging (CMCI). Thank you to Robert Carson and the teaching labs for lending me a high-resolution Leica ICC50W microscope to carry out and monitor my cell survival assays.

I am incredibly grateful to all members of the Zerges lab, past and present, for all their help: Dr. James Dhaliwal, Dr. Shiva Bakhtiari, Brandon Jaunky, Melanie Alfonso, and Dr. Srikanth Tirumani. Whether it be training me or simply lending an ear to my troubleshooting issues, I sincerely appreciate your feedback, our candid conversations, and the kindness you've shown me throughout my graduate studies. I could not imagine my time in the lab without each one of you.

Last but certainly not least, thank you to my friends and family for their steadfast love and support on my academic journey. I dedicate this thesis to my parents, Fiorenza and Renato, and my partner, Brian. Thank you for always encouraging me to be the best that I can be. Making you proud is the greatest reward of all.

Table of Contents

List of Figures

List of Abbreviations

FISH	Fluorescence *in situ* hybridization
HSM	High Salt minimal medium
H_2O_2	Hydrogen peroxide
ROS	Reactive Oxygen Species
Rubisco	Ribulose-1,5-bisphosphate carboxylase/oxygenase
rpm	Rotations Per Minute
rbcL	chloroplast gene encoding the Rubisco Large subunit
rbcS	nuclear gene encoding the Rubisco Small subunit
TAP	Tris-Acetate Phosphate
TE	Tris-Ethylenediaminetetraacetic acid (Tris-EDTA)
DAPI	4′,6-diamidino-2-phenylindole

Chapter 1: Introduction

1.1 Reactive oxygen species (ROS) homeostasis in photosynthetic organisms

Organisms respond to changing biotic and abiotic factors for homeostasis. These acclimation responses are especially important when conditions are extreme and can lead to unmanageable levels of damage and disruption of physiology, *i.e.*, stress. Common to many types of stress and acclimation to stress are reactive oxygen species (ROS).

ROS are unstable, chemical radicals that are produced by all aerobic organisms. They are generated primarily by metabolic reactions in organelles such as chloroplasts, mitochondria, peroxisomes, and the endoplasmic reticulum (Das & Roychoudhury, 2014). The most common types of ROS in cells are superoxide (O_2^-), hydroxyl radicals (OH•), hydrogen peroxide (H_2O_2) and singlet oxygen ($^1O_2$) (Aldred *et al.*, 2009; Foyer & Noctor, 2009).

ROS are generated by the activation of molecular oxygen (O_2). Depending on the ROS, there are two general mechanisms by which this activation occurs (Aldred *et al.*, 2009). The first mechanism involves the absorption of excitation energy, ultimately resulting in excitation of electrons to form singlet oxygen. When singlet oxygen returns to the ground state, it can oxidize another molecule, thereby damaging it. The second mechanism occurs when oxygen gains an additional electron (*i.e.*, is reduced to an oxygen radical) and therefore will have an unpaired electron. These ROS include superoxide and the hydroxyl radical. All three of these ROS have extremely short lifetimes, *i.e.*, they decay rapidly. While the ROS H_2O_2 is not a free radical or an excited form (its electrons are paired), it can be converted to the hydroxyl radical in reactions catalyzed by redox-active iron or other metals in Fenton chemistry (Winterbourn, 2013). Moreover, H_2O_2 is relatively chemically stable, is capable of permeating membranes and can ultimately cause oxidative damage far from its initial origin (Bienert *et al.*, 2006; Winterbourn,

2013). Therefore, a common way to induce oxidative stress is to expose cells to exogenous H_2O_2 (Barone *et al.*, 2021; Blaby *et al.*, 2015), as I have done in Chapter 3 of this thesis.

1.2 Oxidative stress versus antioxidant mechanisms

ROS homeostasis refers to a fine balance between the generation of ROS and antioxidant mechanisms (Foyer & Noctor, 2009). Excessive formation of ROS due to abiotic stresses can cause cellular damage to DNA, proteins, and RNA, rendering them toxic, non-functional or both (Gill & Tuteja, 2010; Li *et al.*, 2006). The production of excess ROS is known as oxidative stress. Oxidative stress occurs when cellular redox homeostasis is disrupted due to the production of ROS that exceeds the rate at which antioxidant responses can control their level, or the level of oxidative damage in a cell (Ray *et al.*, 2012). Since photosynthesis produces an abundance of ROS in the electron transport chain from high light exposure and other stressors, it is vital that photosynthetic organisms develop mechanisms to control ROS overproduction (Foyer & Shigeoka, 2011).

Interestingly, ROS also play beneficial roles as signaling molecules that moderate cell growth and trigger numerous antioxidant responses to mitigate their production and oxidative damage (Foyer & Shigeoka, 2011). One of these antioxidant responses are ROS scavengers, such as ascorbate and glutathione, which not only quench ROS generated from the photosynthetic machinery, but also play a role in controlling gene expression (Foyer & Noctor, 2005, 2009). Another antioxidant mechanism is the detoxification of these ROS by enzymes. Superoxide is detoxified by conversion to H_2O_2 via superoxide dismutase, which is subsequently converted to water and oxygen by catalase (Asada, 2000; Nandi *et al.*, 2019). Additionally, antioxidant enzymes such as glutathione peroxidase, glutathione reductase and methionine sulfoxide reductase repair biological molecules that have been damaged by ROS in mammalian cells (Chatterjee, 2013; Kim,

2013; Santos-Sánchez *et al.*, 2019)**.** Maintaining this balance between ROS production and ROS management is critical, as an abundance of ROS due to stress leads to the oxidation and damage of biological molecules (Gill & Tuteja, 2010; Li *et al.*, 2006).

1.3 Oxidative damage to RNA and its handling

Although much is known about DNA and proteins as being major targets of oxidative damage by ROS, oxidative damage to RNA has been studied less, and relatively little is known about its importance or the antioxidant mechanisms dedicated to it (Li *et al.*, 2006; Wurtmann & Wolin, 2009). It is known that proteins can undergo oxidative modifications that are reversible and aid in redox signaling, whereas modifications that are irreversible can lead to total loss of protein function and degradation of the protein (Davies *et al.*, 1999; McDonagh, 2017). Furthermore, the oxidation of DNA may engender mutations with deleterious phenotypes, the loss of genome stability and impair DNA replication or gene expression (Afshana *et al.*, 2021; Hu *et al.*, 2016).

Like DNA and proteins, RNA can be oxidized. In recent years, new evidence revealed that RNA oxidation is involved in aging and certain neurodegenerative diseases (Liu *et al.*, 2020; Wurtmann & Wolin, 2009). For example, it was found that neurons with elevated RNA oxidation were more likely to develop into Alzheimer's, Parkinson's, or other brain disorders (Nunomura *et al.*, 2009). Other consequences of oxidative damage to RNA, particularly to messenger RNAs (mRNAs), is the production of non-native proteins that can aggregate and cause the stalling of translating ribosomes (Simms *et al.*, 2014).

The handling of oxidized RNA has been proposed to occur in cytoplasmic membrane-less organelles called RNA granules which include stress granules and processing bodies (Buchan &

Parker, 2009; Wurtmann & Wolin, 2009). The yeast *Saccharomyces cerevisiae* has cytoplasmic structures called oxidized RNA bodies (ORBs), which have the translation quality control system called "No-Go decay"; a system that identifies and clears oxidized mRNA (Dhaliwal *et al.*, 2022). Additionally, results using human (HeLa) cells under stress showed that oxidized RNA localized to cytoplasmic ORBs that were separate from stress granules and processing bodies (Zhan *et al.*, 2015). Despite the importance of quality control pathways in the mitigation of oxidized RNA damage, the precise mechanism remains unknown. It is important to understand RNA quality control systems in as many different contexts as possible for comparison studies to understand how this model works.

1.4 The green alga *Chlamydomonas reinhardtii* as a model organism

My thesis work studies these processes in the chloroplast of the green alga *Chlamydomonas reinhardtii* (hereafter "*Chlamydomonas*"). Chloroplasts are the plastid type in photosynthetic tissues of plants and algae and have their own independent genome from which RNAs are transcribed. This genome is the remnant of an ancestral photosynthetic cyanobacterium that was acquired by endosymbiosis billions of years ago, ultimately founding the green lineage (Archibald, 2009).

Chlamydomonas has been used for genetic studies since the early 1900s, and it was only in the 1950s when the first mutants were obtained that *Chlamydomonas* began to be used as a model organism (Harris, 2001). This model organism is used in research to study an array of cellular processes such as chloroplast biology, thylakoid membrane biology and photosynthesis (Harris, 2001). *Chlamydomonas* is also an excellent system to study stress responses, from high light and heat, to nutrient deprivation (Harris, 2001). Since *Chlamydomonas* can grow vegetatively as a

haploid cell, any mutations introduced can be immediately and easily observed through its phenotype (Harris, 2001; Sasso *et al.*, 2018). Furthermore, *Chlamydomonas* can sexually reproduce, meaning it can be crossed to incorporate many characteristics into a single strain and carry out genetic analyses (Sasso *et al.*, 2018). Numerous mutants have been isolated and studied over the years and can be bought from a stock center. Important for this thesis work, *Chlamydomonas* can grow in the dark on medium that has been supplemented with an external carbon source (acetate), all while retaining its photosynthetic properties (Harris, 2001). Due to this, light-sensitive photosynthesis mutants can be studied as well (Spreitzer & Mets, 1981).

Chlamydomonas has a stereotypical intracellular organization of its organelles which make it perfect for mRNA and protein localization experiments (Figure 1). Mitochondria can be found throughout the cytoplasm, as well as between the chloroplast and plasma membrane (Nickelsen & Kück, 2000). A wild-type cell is about 10-12 μm in length and contains a single chloroplast that takes up about 66% of the cell's volume (Harris, 2001).

1.5 The large subunit of Rubisco, RbcL, in chloroplast stress granules

This thesis focuses on an alternate or "moonlighting" role of a photosynthesis protein found during oxidative stress in the chloroplast of *Chlamydomonas*. This project began when under conditions associated with oxidative stress, chloroplast mRNAs localized to foci at the perimeter of the pyrenoid (Uniacke & Zerges, 2008). The pyrenoid is a membrane-less organelle within the chloroplast of most algae and the hornworts and the primary location for the assimilation of carbon dioxide (CO_2) in the Calvin-Benson cycle (Freeman Rosenzweig *et al.*, 2017; Zhan *et al.*, 2018). These foci were termed "chloroplast stress granules" because they shared properties with cytoplasmic stress granules (Kedersha *et al.*, 1999; Mazroui *et al.*, 2006). For example, these

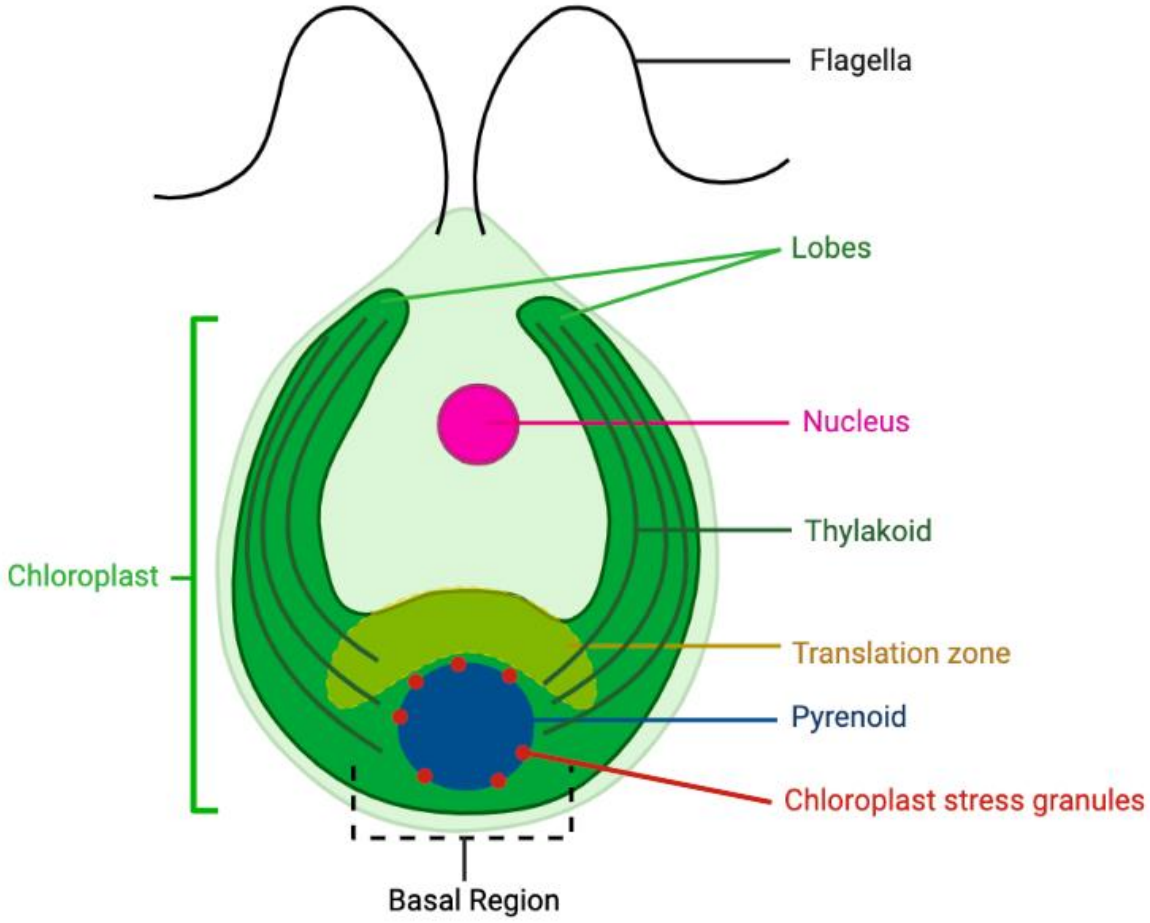

Figure 1. An illustration of a *Chlamydomonas reinhardtii* cell.

The alga cell contains two flagella (in black) for motility. Within the cell is a single cup-shaped chloroplast that contains the aqueous stroma and thylakoid membranes (in dark green). The basal region of the chloroplast encompasses the translation zone (in yellow) and the pyrenoid (in blue) with chloroplast stress granules (in red). The cytoplasm (in pale green) houses the nucleus (in pink). This figure was generated with Biorender.

chloroplast stress granules were found to form under oxidative stress conditions, were enriched in the small ribosomal subunit of 30S but not the large ribosomal subunit of 50S, and they contained a poly(A)-binding protein (Uniacke & Zerges, 2008).

My thesis originated with the finding that chloroplast stress granules also have the large subunit of ribulose-1,5-bisphosphate carboxylase/oxygenase (Rubisco), an enzymatic complex in the Calvin-Benson cycle (Figure 2A). Present in the Rubisco holoenzyme complex are eight copies each of the large subunit (RbcL; Figure 2B) and the small subunit (RbcS) (Spreitzer, 1993). It was postulated that RbcL also has a role in the management of mRNAs from the plastid genome during oxidative stress because 1) this protein has a cryptic RNA binding activity (Yosef *et al.*, 2004) which is activated when it is not assembled in the Rubisco holoenzyme complex and specifically under oxidizing conditions and 2) chloroplast stress granules were not similarly enriched in the small subunit (RbcS) (Uniacke & Zerges, 2008).

This evidence showed that chloroplast stress granules were enriched in a non-Rubisco RbcL, meaning that this form of RbcL has a non-photosynthetic role, and is possibly required to control the level of oxidized RNA (Uniacke & Zerges, 2008). A model was proposed that chloroplast stress granule formation results from Rubisco disassembly which releases RbcL, activates RNA-binding activity under oxidizing conditions and binds RNA at the openings of the pyrenoid tubules (Uniacke & Zerges, 2008, 2009). RbcL shares similarities with stress granule factors as they can both bind non-specifically to mRNA and aggregate during oxidative stress (Knopf & Shapira, 2005).

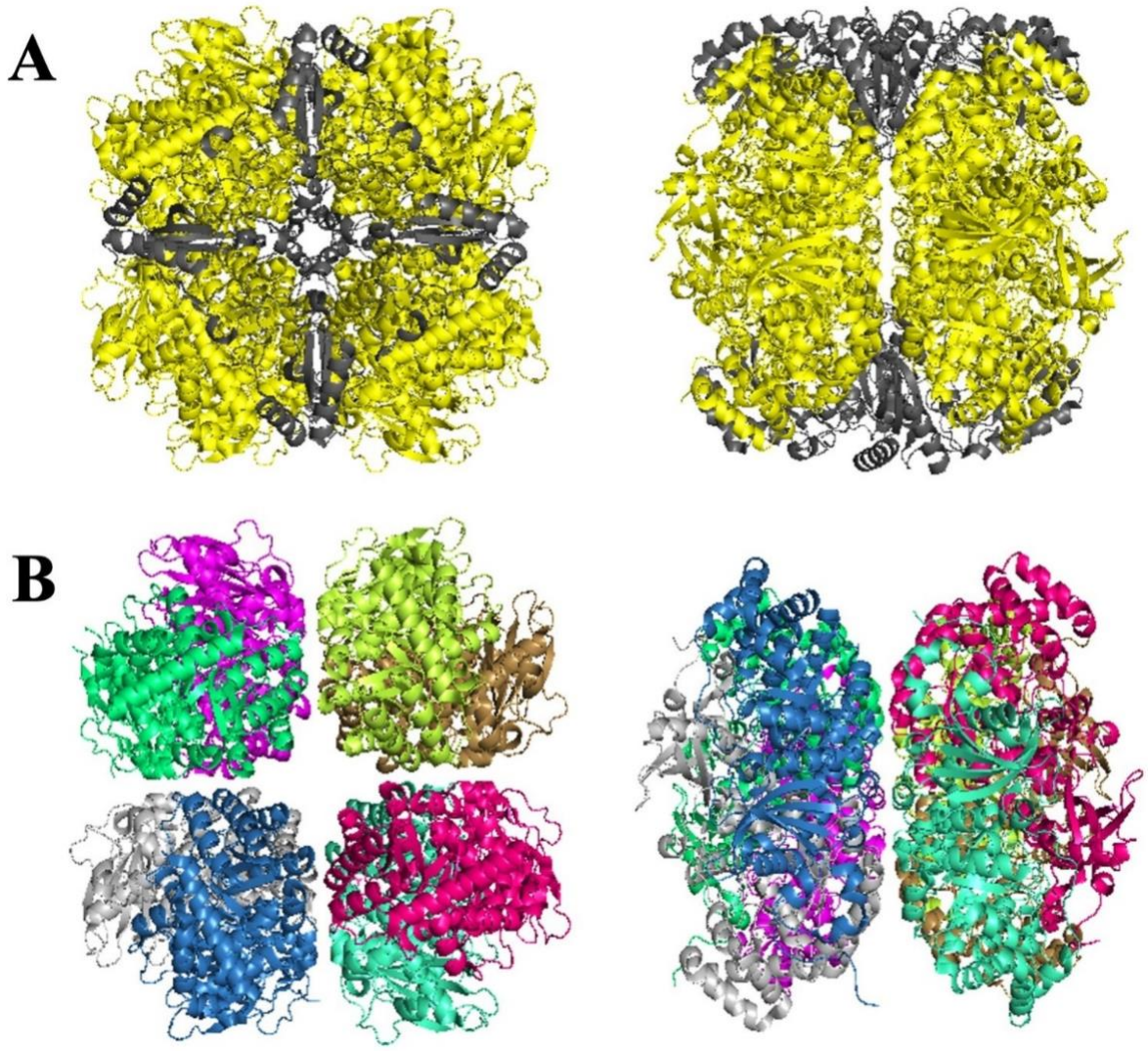

Figure 2. The Rubisco complex and its subunits.

(A) Top and side-view of the Rubisco holoenzyme complex. The large subunits of Rubisco (RbcL) are represented in yellow, whereas the small subunits of Rubisco (RbcS) are represented in grey. (B) Top and side-view of all eight copies of RbcL. Each RbcL subunit is represented by a different color. These figures (*Chlamydomonas reinhardtii* Rubisco, PDB: 1IR2) were generated using PyMol's Schrödinger-LLC program.

1.6 Metabolic enzymes with moonlighting functions as RNA-binding proteins

RbcL fits in a growing class of metabolic proteins that have moonlighting functions as RNA-binding proteins. For example, glyceraldehyde 3-phosphate dehydrogenase (GAPDH) has a primary role in glycolysis breaking down glucose to obtain energy. However, GAPDH can undergo conformational changes and 'moonlight' as an RNA-binding protein, among other functions (Chang *et al.*, 2013; Garcin, 2019). Another example of a metabolic enzyme that moonlights as an RNA-binding protein is aconitase 1. Aconitase 1 has a main function in the citric acid cycle, however when iron levels are unfavorable, it undergoes a structural change and can bind mRNA (Liu & Jeffery, 2020).

Indeed, RbcL has a role in autoregulatory feedback repression of the translation of the chloroplast *rbcL* mRNA encoding it (Wietrzynski *et al.*, 2021). One function of this is in response to oxidative stress. RbcL was found to have an RNA-binding domain, a common occurrence among RNA-binding proteins (Yosef *et al.*, 2004). It is hypothesized that when the Rubisco holoenzyme disassembles during oxidative stress, leading to the degradation of RbcS and the creation of RbcL aggregates, the RNA-binding domain of RbcL located at the N-terminus is exposed to the surface, binding RNA (Knopf & Shapira, 2005; Yosef *et al.*, 2004).

1.7 RbcL and the pyrenoid in the management of oxidized RNA

Research revealed that RbcL and the pyrenoid have roles in the management of oxidized RNA (Zhan *et al.*, 2018). In *Chlamydomonas*, it was found that oxidized RNA accumulated in the pyrenoid (Zhan *et al.*, 2015). The pyrenoid proteome was found to have enzymes in RNA metabolism, including Xrn1 which is required for the clearance of oxidized RNA in *Saccharomyces* (Zhan *et al.*, 2018).

Our laboratory found that RbcL was needed for tolerance to oxidative stress induced by hydrogen peroxide as a mutant lacking RbcS (Δ*rbcS*), and consequently Rubisco, showed elevated tolerance relative to wild-type (Zhan *et al.*, 2015). Additionally, the RbcL that carries out this secondary "moonlighting" function was attributed to a minor pool with distinct physiochemical properties (Zhan *et al.*, 2015). Unlike Rubisco, which is soluble, a minor fraction of RbcL was insoluble even in the presence of non-ionic detergent (Triton X-100) and lacked RbcS, revealing that it was not in Rubisco (Zhan *et al.*, 2015). Previous reports have also demonstrated that under stress in plants and algae, RbcL becomes insoluble due its membrane association (Marín-Navarro & Moreno, 2006; Zhan *et al.*, 2015). Additionally, oxidized RNA was not detected in chloroplast stress granules, however, possibly because it is degraded once localized there (Zhan *et al.*, 2015).

1.8 Thesis overview

This project addressed four goals: 1) to identify if there is a supramolecular state of RbcL that is required in carrying out its moonlighting function under stress; 2) to determine whether specific amino acid residues and other regions of RbcL are involved in stress tolerance; 3) to analyze the biochemical properties of a select group of RbcL mutants obtained from objectives 1 and 2; and 4) to discover where the non-Rubisco form localizes in cells.

To achieve my first goal, I tested supramolecular states of RbcL and their oxidative stress tolerance. RbcL can exist in different supramolecular states; a monomer, a dimer, an octamer and the holoenzyme complex (Wietrzynski *et al.*, 2021). It should be noted that the elevated tolerance seen in the Δ*rbcS* mutant strain likely represents a gain-of-function phenotype because the Δ*rbcL* mutant phenotype was shown to be of low tolerance to H_2O_2. As was shown previously, the *rbcS*

null mutant strain had elevated tolerance and retained the Triton X-100 insoluble RbcL pool (Zhan *et al.*, 2015).

To achieve my second goal, RbcL mutants ordered from a *Chlamydomonas* stock center were made using site-directed mutagenesis to generate amino acid residue substitutions located in the RNA-binding domain of RbcL. These variants (*rbcL-M42V, rbcL-C53A, rbcL-G54D* and *rbcL-P89R*) were analyzed to see what effects they had on oxidative stress response. This will test the role of the RNA-binding domain on the moonlighting function of RbcL in H_2O_2 tolerance. Other site-directed mutants, *rbcL-R217S* (Thow *et al.*, 1994) and *rbcL-V331T* (Chen & Spreitzer, 1989), were also analyzed based on their inability to assemble the Rubisco holoenzyme or altered catalytic activities respectively. Furthermore, it is hypothesized that the properties of this non-Rubisco form of RbcL (such as holoenzyme disassembly, RbcL aggregates, RNA-binding activity) may be regulated by the reversible oxidation of select cysteine residues (García-Murria *et al.*, 2018; Marín-Navarro & Moreno, 2006; Moreno *et al.*, 2008). Therefore, I analyzed some of the conserved cysteine mutants: *rbcL-C84S*, *rbcL-C172S, rbcL-C192S/Y226L, rbcL-C247S* and *rbcL-C449S/C459S.* Not all cysteine mutant residues from the *Chlamydomonas* Resource Center could be tested due to limited supply. Additionally, some of these cysteines have already been analyzed (stress tolerance and insoluble RbcL fractions) previously but are included in the 'Results' section. Not much literature is available for some of the mutants listed above, however, RbcL has been extensively studied in *Chlamydomonas* for its role in Rubisco and, therefore, many mutants have been generated and are available at the stock center.

To achieve the third goal, I used a previously developed subcellular fractionation technique for *Chlamydomonas* cell lysates (Zhan *et al.*, 2015) to analyze whether there was a correlation between the enhanced stress tolerance and the insoluble RbcL pool. For the final goal, I used

immunofluorescence microscopy to localize RbcL in mutants that showed both elevated oxidative stress tolerance and an excess, insoluble RbcL pool in the subfractionation experiments.

Chapter 2: Materials and Methods

2.1 Maintenance of *Chlamydomonas* strains and growth conditions

All strains used throughout this project are listed in Supplementary Tables 1 & 2 (Appendix I). Site-directed mutants were from the *Chlamydomonas* Resource Center (www.chlamycollection.org), whereas supramolecular state mutants were provided by Dr. Katia Wostrikoff, Sorbonne Université (Wietrzynski *et al.*, 2021). All strains were maintained on agar-solidified Tris-acetate phosphate (TAP) medium wrapped in one layer of aluminum foil as Rubisco mutants are extremely light-sensitive (Harris, 1989; Johnson, 2011). All cell cultures used for the survival tests and microscopy experiments were grown in TAP medium under heterotrophic (dark) conditions to mid-logarithmic phase (2-4 x 10^6 cells/ml) with orbital shaking (150 rpm) at 24^{o}C (Harris, 1989). Mutant strains were tested on High Salt minimal (HSM) medium to determine photoautotrophic growth (Harris, 1989) (Supplementary Figure 1, Appendix I).

2.2 Verification of *rbcL* mutant alleles

Prior to use of *rbcL* mutant strains in experiments, the presence of the correct *rbcL* allele in each was verified using polymerase chain reaction (PCR) and DNA sequencing. Template DNA from each mutant strain was amplified by colony PCR (Cao *et al.*, 2009). The oligonucleotides 5' AAGTAAACTGCGTAAGACGA 3' (forward) and 5' GATTGGTTTAGCGGATGATG 3' (reverse) were designed on Benchling (benchling.com) to obtain the amplicons for each site-directed mutant and wild-type strain 2137. The forward oligonucleotide anneals to the 5'UTR of the *rbcL* gene while the reverse oligonucleotide anneals downstream to the 3'UTR region of the gene (Supplementary Figure 2, Appendix I). PCR was conducted on a Veriti 96-well thermal cycler (Applied Biosystems). The thermal cycling program used to obtain the site-directed

amplicons was made up of two rounds of amplification. Round 1 involved 10 cycles of touchdown PCR where the annealing temperature was set higher than the Tm of the oligonucleotides, and steadily lowers after each cycle until it reaches the desired Tm value (or slightly below it) (Green & Sambrook, 2018). The thermal cycler conditions were as follows: 2 min at 94°C for initial denaturation, 30 s at 94°C for denaturation, 30 s at 55 °C → 45 °C for annealing, 30 s at 72°C for extension and lastly 5 min at 72°C for the final extension. The annealing temperature was programmed to decrease by 1°C every cycle until 45°C was reached. Round 2 involved the same amplification and extension steps, however the final annealing temperature (45 °C) from Round 1 was kept for the remaining 20 cycles. This yielded 1.94 kb amplicons as expected except in the case of the *rbcL* deletion mutant *ΔrbcL-MX3312* (Supplementary Figure 3, Appendix I), where a smaller 1.5 kb amplicon will be obtained as the gene is replaced with an *aadA* cassette (Satagopan & Spreitzer, 2004; Zhu *et al.*, 2010).

To verify the supramolecular state mutant L2 and L8 amplicons, oligonucleotides CrRbcLmut: 5' TGAAGAATGTGGTGCTGCTG 3' (forward), and dR-LS.R2: 5' AGAGTACCACCACCGAACTG 3' (reverse) (oligonucleotide sequences provided by Katia Wostrikoff) were used. Additionally, the ΔR T1.3 amplicon was obtained using dR-LS.F: 5' AAGTTTATGACGCCGATTGC 3' (forward) and dR-LS.R2 listed above. The thermal cycler was programmed as follows: 2 min at 94°C for initial denaturation, followed by 35 cycles of 30 s at 94°C for denaturation, 45 s at 53°C for annealing, 30 s at 72°C for extension and 5 min at 72°C for final extension. GeneRuler 1kb Plus DNA ladder (ThermoFisher, SM1331) and amplicons were resolved on a 1% (w/v) agarose gel containing ethidium bromide in 0.5X TBE buffer (Sambrook & Russell, 2001a).

To confirm the presence of amplicons, the bands in the gel were visualized under UV light using a UVP Dual-Intensity Transilluminator. PCR products were then gel extracted and purified using the Monarch DNA Gel Extraction Kit (#T1020G). To ascertain the mutant genotypes, the purified DNA samples were sent for Sanger sequencing to Génome Québec Nanuq. Benchling biology software (benchling.com) was used to verify the FASTA files and confirm the desired mutations.

2.3 Genetic backcrosses and tetrad dissection

To remove any genetic modifiers that affect tolerance, the key *rbcL* mutant strain (CC-4791, *rbcL-G54D,* mating type +) was backcrossed twice to a wild-type strain (CC-124, mating type -). The chloroplast genome is uniparentally inherited from the mating type + parent, whereas the nuclear genome follows Mendelian inheritance (Harris, 1989). As *rbcL* is in the chloroplast genome, the *rbcL-G54D* allele will be transmitted to all progeny in the backcrosses, and they can be phenotypically screened for their inability to grow photoautotrophically.

Genetic crosses and tetrad dissection were carried out as described with a few modifications (Harris, 1989; Jiang & Stern, 2009). All glassware was cleaned, and liquid media was prepared with HPLC-grade water, and the strains were transferred to fresh agar-solidified every three days on TAP plates until ready to be mated. Each strain to be crossed was inoculated using a wire loop in 5 ml of TAP-N liquid medium and the flasks were incubated on a shaker (140 rpm) for 2 hours under high light (Jiang & Stern, 2009). A small aliquot of each culture (strain) was mixed and verified under a light microscope for mating. Then, 2 ml of each culture was mixed in a sterile 10 ml flask and incubated in the dark for 3 hours. Following this, an elongated puddle (no greater than a razor blade in width) of the strain mixture was aliquoted to a Petri plate with TAP medium

solidified with 4% agar, which had been rinsed several times with deionized water prior to addition to the TAP medium. Once the liquid dried, the plates were wrapped in aluminum foil and left for 7 days at 24 ^{o}C to achieve zygote maturation. Vegetative cells were scraped off by passage of a clean razor blade and any that remained were killed by exposure to chloroform for 40 seconds, leaving only zygotes on the agar plates. Tetrad dissection was done under a dissecting microscope and haploid daughter cells were separated as described previously (Jiang & Stern, 2009). The resulting progeny were verified for their inability to grow photoautotrophically on HSM medium. Colony PCR analysis was done to test the mating type of the progeny as seen in Supplementary Figure 4 of Appendix I (Zamora *et al.*, 2004). The progeny of mating type + were then selected once more for a second round of backcrosses.

2.4 Oxidative stress tolerance test (Trypan Blue exclusion assay)

To select *rbcL* mutants that exhibit high cell survival to oxidative stress, 20 ml cultures of each strain were exposed to 4 mM H_2O_2 and monitored at time points of 0, 2 and 4 hours (Dhaliwal, 2021). A dye-exclusion assay using Trypan Blue (Sigma-Aldrich #T8154) was employed to determine cell survival (Strober, 2015). Cells were counted using either the color camera DsRi2 CMOS of a Nikon Eclipse TiE inverted epifluorescence microscope (20x bright lens) or a high-resolution Leica ICC50W light microscope (40x objective lens). For statistical analyses, at least three biological replicate experiments were performed using independent cultures of each strain, and the mean survival rates were compared using unpaired two sample t-tests ($p \leq 0.05$).

2.5 Indirect immunofluorescence staining and microscopy

Immunofluorescence staining was conducted as described previously (Uniacke *et al.*, 2011). The slides were incubated with rabbit antibodies against: RbcL (Dr. Robert Spreitzer, dilution 1:100), S-21 (α30S chloroplast ribosomal protein, (Randolph-Anderson *et al.*, 1989), dilution 1:1000) and EPYC1 (Agrisera AS194312, dilution 1:1000). The primary antibodies were left overnight at 4°C. DAPI (4′,6-diamidino-2-phenylindole) (dilution 1:1000) was also used to stain nuclear bodies within *Chlamydomonas* cells before the addition of Antifade mounting medium.

The secondary antibodies used were Alexa-Fluor-488 and Alexa-Fluor-568, both conjugated to goat anti-rabbit IgG antibodies (Invitrogen Inc.). Microscopy images were obtained with a Leica DMI6000B inverted epifluorescence microscope using a Hamamatsu Orca R2 CCD camera. A 63x/1.4 NA objective lens in addition to a 1.6x magnification tube lens was utilized. The images were captured with a Z-stack spacing of 0.2 μm per section in DAPI, GFP, Texas Red, brightfield (BF) and differential interference contrast (DIC) channels and visualized using Volocity acquisition software (Perkin-Elmer). When required, images were deconvoluted with AutoQuant X3 (Media Cybernetics Inc.).

2.6 Fluorescence *in situ* hybridization (FISH)

The *psbA* mRNA primary probe design and FISH protocol used here were described previously (Bakhtiari Koohsorkhi, 2021; Tsanov *et al.*, 2016) with the following modifications: the hybridization mix contained 10% dextran sulfate, 2x saline-sodium citrate (SSC), and 10% formamide (v/v) instead of 10.6% dextran sulfate (w/v), 1x SSC, and 15% formamide (v/v) (Wefers *et al.*, 2022). Additionally, the slides were incubated with the hybridization solution at 37 °C for 3 hours in a hybridization oven (Boekel Scientific InSlide Out). Once the slides were washed

in a post-hybridization buffer and phosphate-buffered saline with magnesium (PBS-Mg), 12 µl of Antifade was added. All images were acquired on the Leica DMI6000B inverted epifluorescence microscope in the Texas Red channel.

2.7 Fractionation and immunoblot analyses.

Fractions were attained through differential centrifugation as described previously (Zhan *et al.*, 2015). Cultures were grown in 50 ml of TAP medium in foil-wrapped flasks to a density of 3.5 - 5.5 x 10^6 cells/ml. Aliquots of each fraction were suspended in sodium dodecyl sulfate (SDS)-PAGE loading buffer (250 mM Tris-HCl, pH 6.8; 0.4 g of SDS, 20% glycerol, 20% β-mercaptoethanol, bromophenol blue) before being placed at -80 ^{o}C.

When protein samples were ready to be analyzed, they were denatured by boiling for 5 minutes and equal volume loadings of each fraction were resolved by SDS-PAGE on a 12% acrylamide gel (Sambrook & Russell, 2001b). The protein samples were then transferred overnight at 4 ^{o}C to PVDF membranes (Bio-Rad). Protein on the membrane was stained with Ponceau S solution (Bioshop) before the membranes were blocked with 5% (w/v) skim milk powder in 1X PBS and 0.1% Tween-20. All primary and secondary antibody incubations were also done in 5% skim milk with 1X PBS-Tween. The membranes were reacted in primary antisera against RbcL (Agrisera, AS03037, 1:10,000) and RbcS (Dr. Robert Spreitzer, dilution 1:2000) for 2 hours at room temperature with gentle agitation (50 rpm). Membranes were then incubated in secondary antibody (horseradish peroxidase-conjugated goat anti-rabbit IgG antibody (KPL), 1:10,000) for 1 hour at room temperature with gentle agitation (50 rpm). The membranes were first probed with Pierce ECL Western Blotting Substrate (ThermoFisher) followed by SuperSignal West Pico PLUS Chemiluminescent substrate (ThermoFisher) for ECL detection, and signal intensity was captured

with the Amersham Imager 600 (GE Healthcare Life Sciences). The procedure was repeated once more with primary antisera against S-21 (α30S ribosomal protein, (Randolph-Anderson *et al.*, 1989), dilution 1:30,000). The RbcS blots were harshly stripped before adding blocking solution (protocol can be found here: https://www.abcam.com/protocols/western-blot-membrane-stripping-for-restaining-protocol).

A dilution series was used to show that signals from RbcL and RbcS were in the linear range and to determine their relative levels in the fractions. An initial exposure of 2 minutes was done on the Imager 600 analysis software to obtain RbcL and RbcS ECL signals from supernatant fractions. Following this, incremental exposures of 5 minutes to a maximum total exposure of 25 minutes were used to obtain optimal images of the pellet fractions on the Imager 600. Signals from S-21 were obtained after 2 minutes of auto exposure. For quantification, background signal was removed from the raw signal intensity values of captured images using FIJI software and plotted in Excel to generate signal ratios and graphs.

Chapter 3: Results

3.1 The RbcL dimer may be specifically required for the moonlighting function.

Previously, it has been shown that RbcL that is not in the Rubisco holoenzyme is required for oxidative stress tolerance in *Chlamydomonas* (Zhan *et al.*, 2015). When a Rubisco mutant that lacks *rbcL* (*ΔrbcL*) was subjected to 4 mM H_2O_2 (a reactive oxygen species), it showed lower survival than a wild-type strain (Zhan *et al.*, 2015). Interestingly, a mutant deficient for RbcS (*ΔrbcS*) showed elevated H_2O_2 tolerance relative to wild-type (Zhan *et al.*, 2015). Therefore, it was proposed that the RbcL in the latter strain was more available for the moonlighting function in oxidative stress tolerance. This raised the question regarding the biochemical nature of this RbcL.

RbcL can exist as a monomer, a dimer, an octamer, and a holoenzyme complex (Wietrzynski *et al.*, 2021). A strain carrying *rbcL-E109A/R253A* (hereafter "*L2-mut*") has monomeric RbcL; a strain carrying *rbcL-A143W/R215A/D216A* (hereafter "*L8-mut*") accumulates mainly dimeric RbcL but does also have monomeric RbcL; and a strain carrying Δ*rbcS* contains mostly octameric RbcL, but also has monomeric and dimeric RbcL (Wietrzynski *et al.*, 2021). The octamer (Δ*rbcS*) is known to carry out a moonlighting function by mediating autoregulatory feedback repression of *rbcL* translation when RbcS is limiting for assembly (Wietrzynski *et al.*, 2021). I was interested in determining which supramolecular state of RbcL is responsible for its moonlighting function in oxidative stress tolerance, and whether it is distinct from the aforementioned autoregulatory role.

I tested the provided RbcL supramolecular state mutants (Supplementary Table 2, Appendix I) using a similar experiment as described above, where different strains were subjected to 4 mM H_2O_2 and monitored over the course of 4 hours (Figure 3A) (Zhan *et al.*, 2015). More precisely, strains that have different proportions of the various supramolecular states of RbcL were tested. Dead cells were detected with the Trypan Blue exclusion test if they stained blue, whereas

living cells would remain green (Strober, 2015). The cell survival percentages for each trial and timepoint were divided by the corresponding value at time 0 to ensure an initial survival rate of 100% for all.

Looking at Figure 3B, the CC-125 wild-type is the control strain for the supramolecular states of RbcL, and only assembles Rubisco holoenzyme. Next, in orange, is the strain that has a higher proportion of octameric RbcL (*ΔrbcS*), and it shows *enhanced* oxidative stress as compared to the wild-type strain. On the other hand, the *rbcL* deletion mutant seen in pink shows survival statistically indistinguishable from that of wild-type. A truncated *rbcL* that expresses only the N-terminus of the gene (LS_{tr}) shown in blue conferred wild-type survival. Similarly, the strain that has a higher proportion of monomeric RbcL (*rbcL-L2-mut*) shown in yellow as well as a construct that produces more RbcL than wild-type shown in red (5'*psaA:rbcL*) showed stress tolerance equal to wild-type. Interestingly, the strain that has a higher proportion of dimeric RbcL (*rbcL-L8-mut*) showed elevated oxidative stress tolerance, more so than even *ΔrbcS.*

It should be noted that the elevated tolerance seen in the Δ*rbcS* mutant likely represents a gain-of-function phenotype because the Δ*rbcL* mutant phenotype was shown to have low tolerance to H_2O_2. Therefore, these results support a role of the RbcL dimer in the moonlighting function in oxidative stress tolerance. Moreover, distinct RbcL supramolecular states carry out each of the two moonlighting functions because, as was mentioned above, the autoregulatory feedback repression of *rbcL* translation requires the RbcL octamer (Wietrzynski *et al.*, 2021).

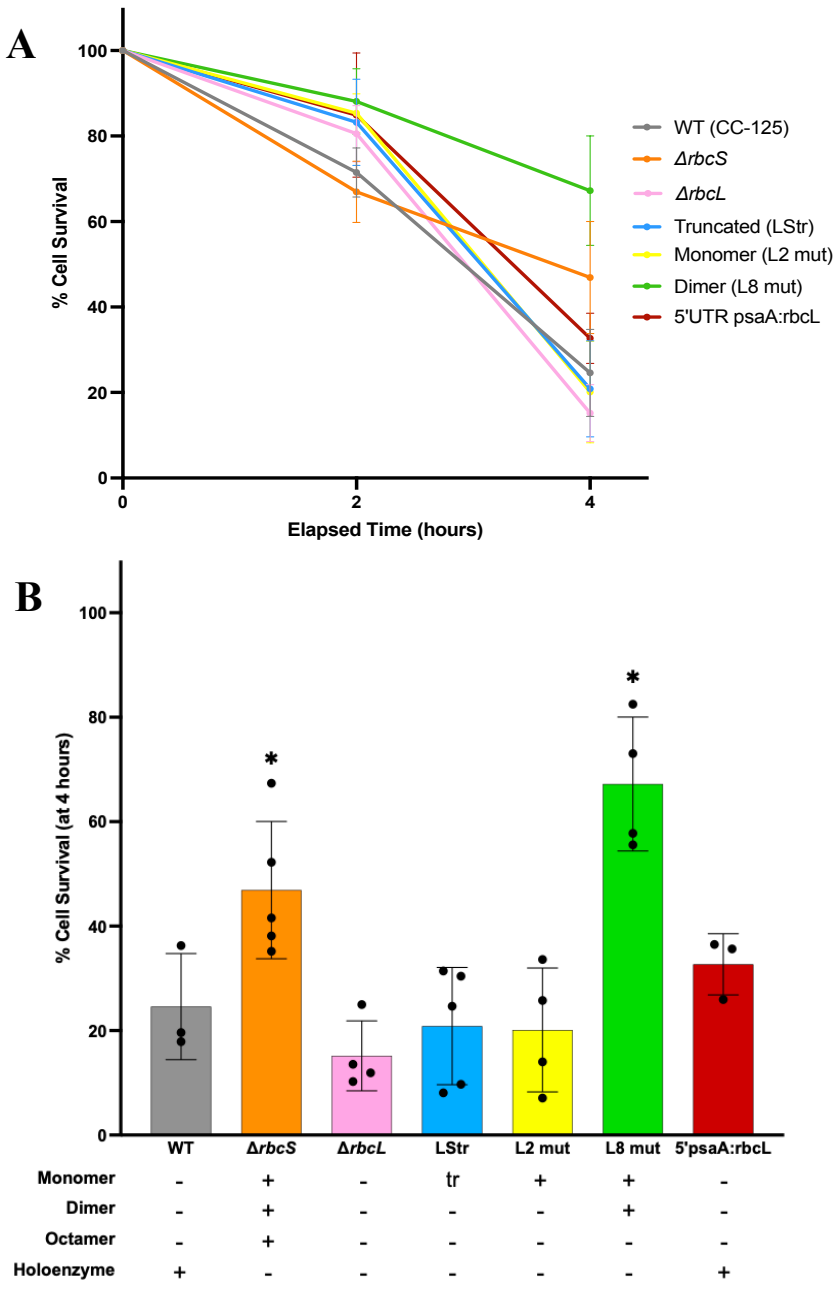

Figure 3. Determining RbcL moonlighting functions in supramolecular state mutants. (A) Mean cell survival rates of supramolecular state mutants exposed to 4 mM H_2O_2, as observed via a time course assay with Trypan blue exclusion test. Cell survival percentages for each trial and timepoint were divided by the corresponding value at time 0 to ensure an initial survival rate of 100%. (B) Bar chart showing results at the 4-hour timepoint from (A). Bar heights indicate the mean percent cell survival; individual points illustrate biological replicates ($n \geq 3$). A plus sign (+) indicates that the supramolecular state of RbcL was detected in that strain (Wietrzynski *et al.*, 2021). LStr expresses truncated RbcL with only the N-terminal region (tr). Asterisks refer to statistical significance in unpaired two-sample Student's t-tests ($p \leq 0.05$).

3.2 Certain conserved cysteine residues and amino acid substitution variants in the RNA-binding domain showed elevated oxidative stress tolerance to H_2O_2.

Our laboratory was also interested in determining if certain regions of the RbcL protein are needed to bring about its moonlighting function, *i.e.*, the disassembly of the holoenzyme, RNA-binding activity and RbcL aggregates (Knopf & Shapira, 2005; Yosef *et al.*, 2004).

As the RNA-binding activity of RbcL was predicted to lie within the first 150 amino acids of the protein (Yosef *et al.*, 2004), *rbcL* alleles with site-directed amino acid substitutions at the N-terminal region (*rbcL-M42V, rbcL-C53A, rbcL-G54D* and *rbcL-P89R*) were selected to be tested. The RNA-binding domain has structural similarity to an RNA recognition motif found in certain RNA-binding proteins, and RbcL which also has this domain was shown to bind RNA *in vitro* (Yosef *et al.*, 2004). The *rbcL-R217S* and *rbcL-G54D* mutants prevent the assembly of the Rubisco holoenzyme (Spreitzer, 1993; Thow *et al.*, 1994). When Rubisco holoenzyme cannot assemble, various supramolecular states of RbcL accumulate, as was seen in the RbcS deficient mutant (Δ*rbcS*) (Wietrzynski *et al.*, 2021). The *rbcL-V331T* mutant was tested to determine whether this residue has a role. It assembles the Rubisco holoenzyme but with impaired catalytic activity (Chen & Spreitzer, 1989).

Furthermore, it is hypothesized that the properties of this alternate form of RbcL under oxidizing conditions (disassembly, aggregates, etc.), may be regulated by the reversible oxidation of certain conserved cysteine residues (García-Murria *et al.*, 2018; Marín-Navarro & Moreno, 2006; Moreno *et al.*, 2008). Therefore, I decided to analyze mutants for most of the conserved cysteine mutants: *rbcL-C84S*, *rbcL-C172S, rbcL-C192S/Y226L, rbcL-C247S, rbcL-C284S* and *rbcL-C449S/C459S. rbcL* mutants for certain cysteine residues were not available from *Chlamydomonas* Resource Center (www.chlamycollection.com). It is important to note that

originally, the strain carrying *rbcL-C192S/Y226L* was initially thought to possess only *rbcL-Y226L,* a mutant that was generated to study Rubisco degradation (Esquível *et al.*, 2006). However, by sequencing this allele, I found that there was an additional mutation, *C192S*. Other cysteine mutants (*rbcL-C84S*, *rbcL-C172S* and *rbcL-C449S/C459S*) as well as *rbcL-G54D* were previously analyzed (Dhaliwal, 2021).

I tested the above-mentioned mutants using the same Trypan Blue exclusion assay described in 3.1 (results seen in Figure 4B). The cell survival percentages for each trial and timepoint were divided by the corresponding value at time 0 to ensure an initial survival rate of 100% for all. Looking at Figure 4C, strains carrying *rbcL-M42V*, *rbcL-G54D, rbcL-C19S/Y226L, rbcL-C247S* and *rbcL-C284S* showed elevated tolerance to H_2O_2 that is statistically significant in comparison to the control strain (wild-type 2137). The results for *rbcL-G54D,* which had been backcrossed (see Materials and Methods) to control for any genetic background effects, were also as seen previously (Dhaliwal, 2021).

Overall, our hypothesis is that the mutants that are exhibiting a higher tolerance, or an *enhanced* tolerance, to H_2O_2 would accumulate the non-Rubisco form of RbcL at higher levels than wild-type strains. More so, these findings give us a clue as to which regions of the protein are possibly involved in this moonlighting RbcL function.

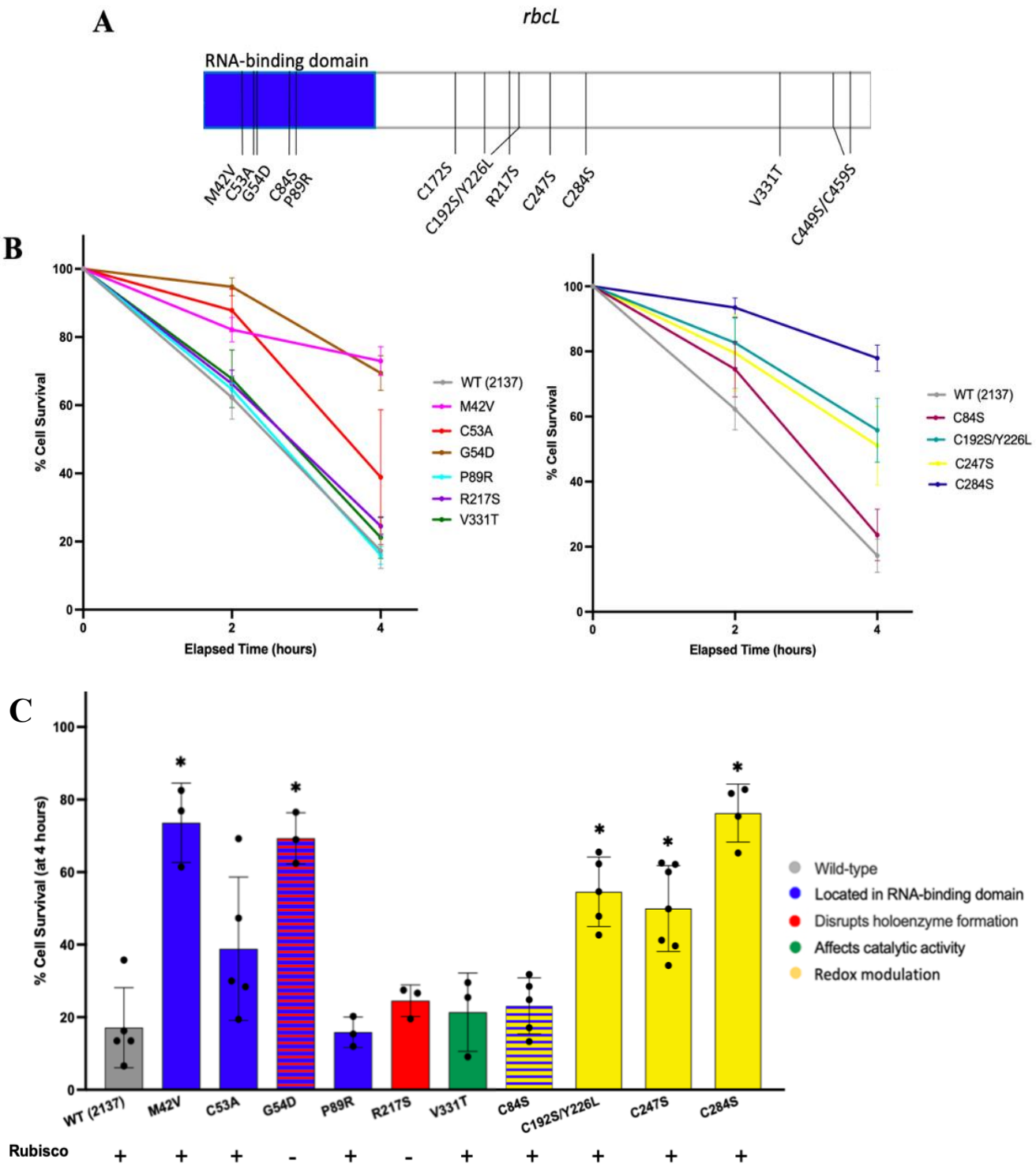
A
rbcL
RNA-binding domain
M42V
C53A
G54D
C84S
P89R
C172S
C192S/Y226L
R217S
C247S
C284S
V331T
C449S/C459S
B
% Cell Survival
Elapsed Time (hours)
WT (2137)
M42V
C53A
G54D
P89R
R217S
V331T
C84S
C192S/Y226L
C247S
C284S
C
% Cell Survival (at 4 hours)
WT (2137)
M42V
C53A
G54D
P89R
R217S
V331T
C84S
C192S/Y226L
C247S
C284S
Rubisco
+ + + - + - + + + + +
Wild-type
Located in RNA-binding domain
Disrupts holoenzyme formation
Affects catalytic activity
Redox modulation

Figure 4. Select site-directed *rbcL* mutants showed elevated tolerance to H_2O_2-induced oxidative stress. (A) The relative positions of all site-directed amino acid substitutions within RbcL. (B) Mean cell survival rates of mutants exposed to 4 mM H_2O_2, as observed via a time course assay with Trypan blue exclusion test. Cell survival percentages for each trial and timepoint were divided by the corresponding value at time 0 to ensure an initial survival rate of 100%. Cysteine-to-serine mutants were grouped together separately from other mutants for better visualization of the data and are shown on the right. (C) Bar chart showing results at the 4-hour timepoint from (B). Bar heights indicate the mean percent cell survival; individual points illustrate biological replicates ($n \geq 3$). Bar color corresponds to how the substitution affects RbcL. A plus sign (+) below a bar identifies strains which exhibit photoautotrophic growth, and therefore have Rubisco. Asterisks refer to statistical significance in unpaired two-sample Student's t-tests ($p \leq 0.05$).

3.3 A partial correlation between stress tolerance and a minor, insoluble form of RbcL in mutants.

Previously, it has been shown that a minor pool of RbcL distinct from the RbcL in the Rubisco holoenzyme and insoluble in Triton X-100 was present in the wild-type and *ΔrbcS* mutant strains (Zhan *et al.*, 2015). The latter result suggested that this pool was responsible for the elevated tolerance to oxidative stress. Therefore, to further explore if there is a relationship between this minor, Triton X-100 insoluble fraction and the moonlighting function of RbcL, a differential centrifugation experiment was conducted as described previously (Zhan *et al.*, 2015). Three fractions were prepared: a supernatant fraction (S16) containing soluble proteins such as Rubisco, a Triton-soluble supernatant (P16-TS) fraction (which was not analyzed in this thesis) and a Triton-insoluble pellet (P16-TI) fraction which has the minor pool of RbcL (Zhan *et al.*, 2015). In previous experiments, no difference in antibody staining on immunoblots was seen between non-stressed samples and H_2O_2 samples, meaning that this pool of RbcL with a moonlighting function must be constitutively present (Zhan *et al.*, 2015). Therefore, I decided to look only at non-stressed cell lysate samples of the site-directed and supramolecular state mutant strains.

As seen in Figure 5A (lane 1), RbcL and RbcS were detected in total protein from the S16 fraction of wild-type 2137 cells. This is as expected as the S16 fraction from wild-type cells contains only Rubisco, a soluble complex with equal stoichiometry of the subunits (Spreitzer & Salvucci, 2002; Wietrzynski *et al.*, 2021; Zhan *et al.*, 2015). As this represents Rubisco in the wild-type S16 fraction, the ratio of the signals (RbcL/RbcS) was designated as 1.0 (1 RbcL:1 RbcS) and the ECL signal ratios from the mutants were corrected accordingly (see table below blots, "RbcL/RbcS"). A dilution series of the wild-type S16 extract was included on each blot (20 µg, 10 µg, 5 µg in Figure 5A; 2.5 µg, 1 µg and 0.33 µg in Figure 5B) to (1) show the RbcL/RbcS ratio

that represents Rubisco and (2) determine whether signals were in the linear range of ECL signal intensity to protein amount. Certain samples (*rbcL-C84S, rbcL-C172S, rbcL-C449S/C459S*) were also prepared and analyzed previously (Dhaliwal, 2021).

One of three replicate experiments is shown here (Figure 5); the others can be found in Appendix I, Supplementary Figure 5. It should be noted that the quantification of these ECL signals is not precise. Abnormalities in some regions of the blots and the signals from the P16-TI fractions were below the standard dilution series of wild-type extract and, therefore, may not have been in the linear range of the signal to protein ratio. Taking this into account, the bands were evaluated qualitatively as well to assess whether for each mutant RbcL or RbcS was in excess (Figure 5B, "Qualitative assessment"). More emphasis was placed on results in immunoblot trials where bands were not affected by abnormalities, like non-specific signal, irregular shaped bands, or blotches possibly representing transfer problems.

The RbcL/RbcS ratio of the soluble S16 fractions from the mutants shows the expected results; those that accumulate Rubisco (grow photoautotrophically; Supplementary Figure 1 in Appendix) had both detectable amounts of RbcL and RbcS as seen in Figure 5A (wild-type, *rbcL-M42V, rbcL-C53A, rbcL-C84S, rbcL-C172S, rbcL-C192S/Y226L, rbcL-C247S, rbcL-C284S, rbcL-C449S/C459S*). Furthermore, the mutants that are known to not accumulate Rubisco (*ΔrbcS, ΔrbcL, rbcL-L2-mut*, *rbcL-L8-mut*, *rbcL-G54D* and *rbcL-R217S*) do not have either subunit detected in the S16 fraction (Wietrzynski *et al.*, 2021; Zhan *et al.*, 2015).

Interestingly, in the P16-TI fractions, this insoluble RbcL pool was observed in both the wild-type and *ΔrbcS,* but not *ΔrbcL* (Zhan *et al.*, 2015). As noted previously, the *rbcS* null mutant had elevated tolerance and retained the Triton X-100 insoluble RbcL pool as expected (Zhan *et al.*, 2015). However, when looking for a pattern amongst the site-directed mutants with high

oxidative stress tolerance and this insoluble RbcL pool; one could not be found. The *ΔrbcS*, *rbcL-L2-mut*, *rbcL-L8-mut*, *rbcL-G54D, rbcL-R217S* and *rbcL-C247S* all accumulated an excess amount of this insoluble RbcL in comparison to its RbcS counterpart (Figure 5B, lanes 2, 5, 8, 9 and 13). However, *rbcL-R217S* and *rbcL-L2-mut* did not show increased cell survival under oxidative stress. Perhaps a certain threshold must be met for this moonlighting function to come about. If the level is too high (in the case of *rbcL-R217S*) or the RbcL does not accumulate above a required amount (*rbcL-L2-mut*), it has the opposite effect. Furthermore, the other amino acid substitutions that also showed elevated tolerance either: 1) accumulated more RbcS, which was the case for *rbcL-M42V*; or 2) had undetectable levels of RbcL and RbcS, as was the case for *rbcL-C284S*.

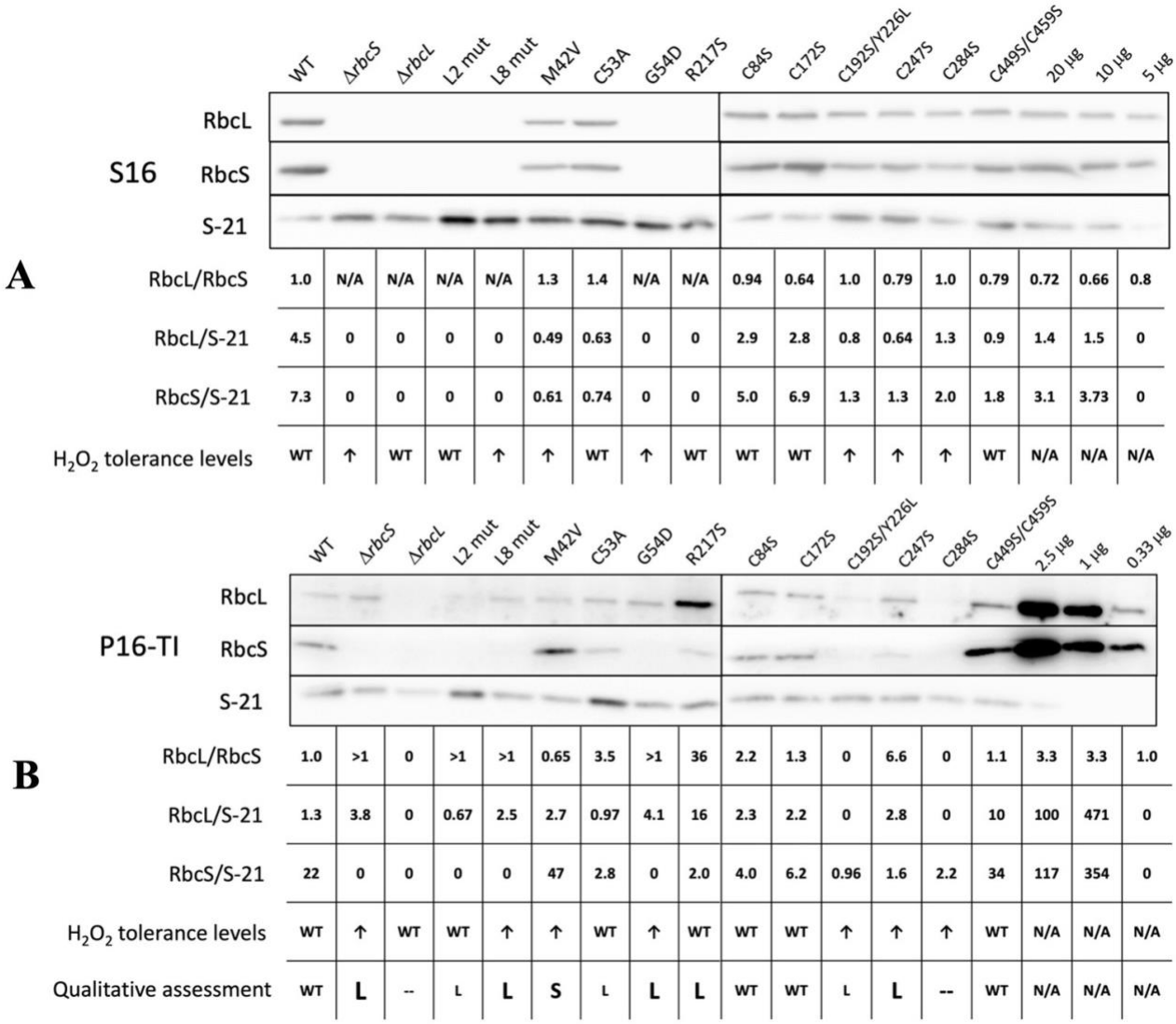
WT
ΔrbcS
ΔrbcL
L2 mut
L8 mut
M42V
C53A
G54D
R217S
C84S
C172S
C192S/Y226L
C247S
C284S
C449S/C459S
20 µg
10 µg
5 µg
RbcL
S16
RbcS
S-21
A
RbcL/RbcS 1.0 N/A N/A N/A N/A 1.3 1.4 N/A N/A 0.94 0.64 1.0 0.79 1.0 0.79 0.72 0.66 0.8
RbcL/S-21 4.5 0 0 0 0 0.49 0.63 0 0 2.9 2.8 0.8 0.64 1.3 0.9 1.4 1.5 0
RbcS/S-21 7.3 0 0 0 0 0.61 0.74 0 0 5.0 6.9 1.3 1.3 2.0 1.8 3.1 3.73 0
H2O2 tolerance levels WT ↑ WT WT ↑ ↑ WT ↑ WT WT WT ↑ ↑ ↑ WT N/A N/A N/A
WT
ΔrbcS
ΔrbcL
L2 mut
L8 mut
M42V
C53A
G54D
R217S
C84S
C172S
C192S/Y226L
C247S
C284S
C449S/C459S
2.5 µg
1 µg
0.33 µg
RbcL
P16-TI
RbcS
S-21
B
RbcL/RbcS 1.0 >1 0 >1 >1 0.65 3.5 >1 36 2.2 1.3 0 6.6 0 1.1 3.3 3.3 1.0
RbcL/S-21 1.3 3.8 0 0.67 2.5 2.7 0.97 4.1 16 2.3 2.2 0 2.8 0 10 100 471 0
RbcS/S-21 22 0 0 0 0 47 2.8 0 2.0 4.0 6.2 0.96 1.6 2.2 34 117 354 0
H2O2 tolerance levels WT ↑ WT WT ↑ ↑ WT ↑ WT WT WT ↑ ↑ ↑ WT N/A N/A N/A
Qualitative assessment WT L -- L L S L L L WT WT L L -- WT N/A N/A N/A

Figure 5. The levels of wild-type and mutant RbcL in soluble and Triton X-100 insoluble forms was determined by immunoblot analysis. (A, B) The supernatant (S16) fraction and the Triton X-100 insoluble pellet (P16-TI) fraction of wild-type and mutants were analyzed by SDS-PAGE and immunoblot analyses. The blots were incubated with antisera raised against RbcL, RbcS and the chloroplast ribosomal protein S-21 as a control for the amount of protein in each lane. A dilution series of the wild-type S16 extract was included on each blot to reveal proportionality of signal to RbcL. Black vertical lines in (A) and (B) indicate joining of blots which were performed and imaged entirely in parallel (*i.e.*, under identical conditions and ECL imager settings and exposures). Blots from (A) were from shorter exposure than the blots from (B) due to the higher concentration of S16 than in the P16-TI fractions. Below each blot is a quantification table of the RbcL to RbcS ratio (RbcL/RbcS), the RbcL to S-21 ratio (RbcL/S-21) and RbcS to S-21 ratio (RbcS/S-21). A '>1' indicates an excess of RbcL relative to wild-type. The H_2O_2 tolerance levels for wild-type and the mutants was indicated as follows: an upwards arrow (↑) refers to enhanced stress tolerance, and 'WT' refers to wild-type levels of stress tolerance. 'L' and 'S' refer to excess RbcL and RbcS, respectively, compared to wild-type, whereas '--' indicated non-detection and 'WT' indicated a wild-type RbcL to RbcS ratio. The font size of the letters indicates the degree of the difference from wild-type.

3.4 RbcL punctate bodies are present throughout the chloroplast of select mutants: *ΔrbcS, rbcL-G54D* and *rbcL-L8-mut.*

Recall that under conditions associated with oxidative stress, chloroplast mRNAs such as *rbcL* localized to foci at the perimeter of the pyrenoid in wild-type cells (Uniacke & Zerges, 2008). We hypothesized that the reason for these visible foci was the disassembly of the Rubisco holoenzyme, releasing RbcL so that it can bind mRNAs and ultimately aggregate, like stress granules. However, the select mutants in this thesis (*ΔrbcS, rbcL-G54D* and *rbcL-L8-mut*) that exhibited enhanced oxidative stress tolerance as well as an excess, insoluble P16-TI fraction, do not assemble Rubisco holoenzyme (Spreitzer, 1993; Wietrzynski *et al.*, 2021).

I then investigated where this non-Rubisco form of RbcL is localizing in the chloroplast of these mutant strains, *i.e.*, is it found in the basal region of the chloroplast, in chloroplast stress granules or in the lobes (Figure 1). I examined this specifically in the strains that exhibited high levels of cell survival during stress as well as an accumulation of the insoluble P16-TI form such as *ΔrbcS, rbcL-G54D* and the *rbcL-L8-mut*. Previous groups have shown that EPYC1 is responsible for linking together Rubiscos that ultimately come together to form the pyrenoid, and co-stains with Rubisco (Mackinder *et al.*, 2016). Therefore, before subjecting the mutants with H_2O_2-induced stress and localizing RbcL, I decided to use EPYC1 on wild-type cells as well as the strain carrying *rbcL-G54D* to verify pyrenoid formation (Supplementary Figure 6 in Appendix I). As expected, wild-type cells stained the pyrenoid as a 'ball', whereas *rbcL-G54D* stained all throughout the chloroplast, indicating the absence of Rubisco in this strain.

Next, I compared no stress (Figure 6A) and 2 mM H_2O_2-induced stress for 1 hour (Figure 6B) in the different RbcL mutants (*ΔrbcS, rbcL-G54D* and *rbcL-L8-mut*). As seen in Figure 6, I used an affinity-purified RbcL antibody (shown in magenta) and DAPI (shown in blue) to label

nuclei and determine the orientation of the cells. In wild-type cells, RbcL localizes to the pyrenoid, as expected (Figure 6A and B, first row). Under stress, chloroplast stress granules can be seen around the pyrenoid in wild-type, but not in all cells (Figure 6B, first row). The strain carrying *ΔrbcL* shows no RbcL signal, which is also expected as it is the negative control (Figure 6A and B, second row). Interestingly, *ΔrbcS, rbcL-G54D* and *rbcL-L8-mut* all showed constitutively present RbcL aggregates or punctate bodies, regardless of stress. As seen here, it was previously shown that *rbcL-G54D* formed foci all throughout the chloroplast and were also constitutively present (Dhaliwal, 2021). There does not seem to be a specific location for these punctate RbcL bodies as some appear to be in the chloroplast lobes and the basal region of the chloroplast. Furthermore, these RbcL punctate bodies are present in most, but not all, of the cells. However, it can be said that these punctate RbcL bodies accumulate specifically the insoluble form of RbcL seen in the previous section of this thesis (Results; 3.3). The presence of these RbcL punctate structures, or foci, may play a role in the moonlighting function of RbcL and its overall tolerance to oxidative stress.

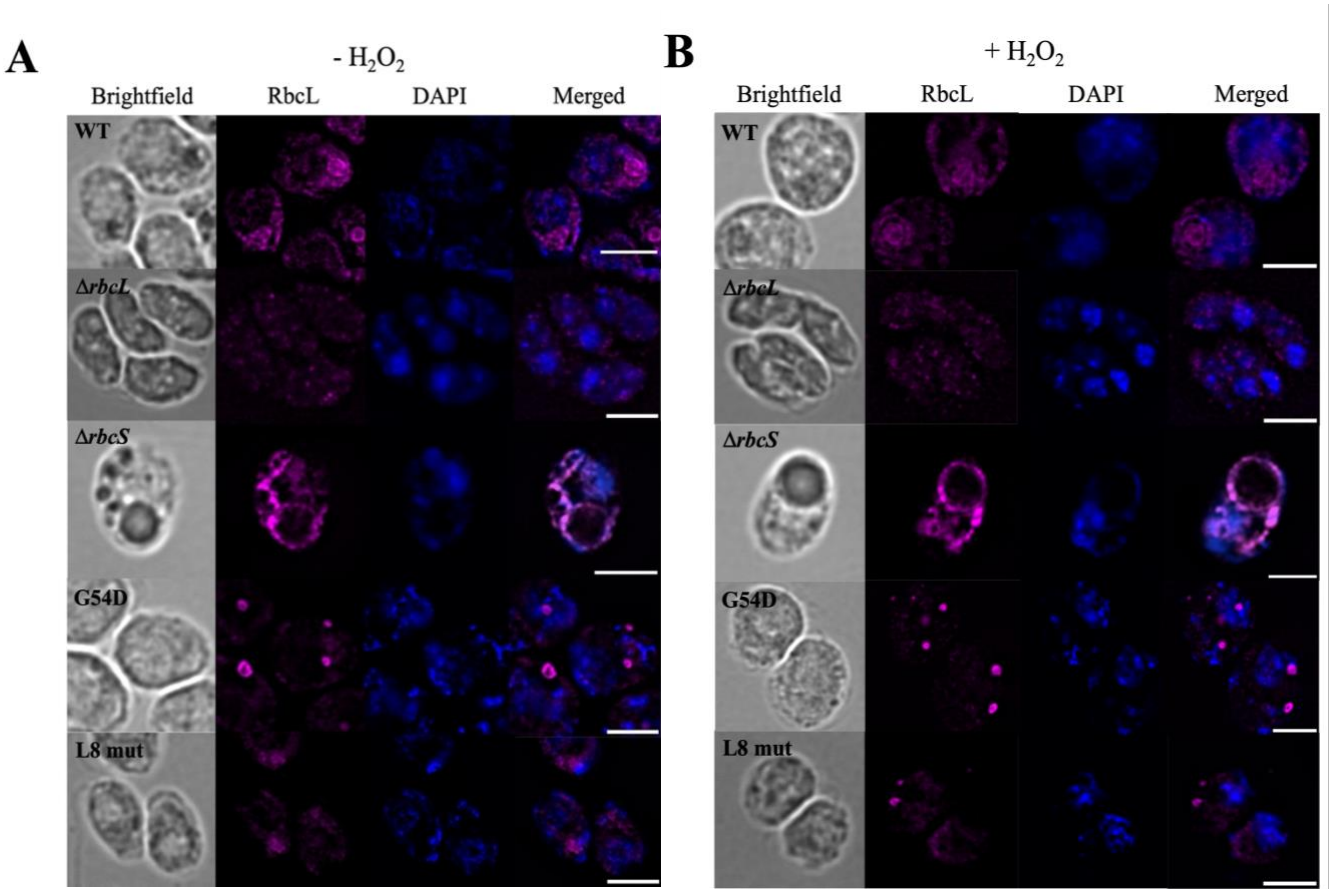

Figure 6. Immunofluorescence staining of RbcL in key mutants. Immunofluorescence signals of RbcL (in magenta) and DAPI (in blue) were acquired and merged. Wild-type and mutant strains (*ΔrbcS, ΔrbcL, rbcL-G54D* and *rbcL-L8-mut*) were analyzed under (A) non-stress and (B) stress conditions (2 mM H_2O_2 for 1 hour). Scale bars indicate 5 μm in length.

Chapter 4: Discussion

The results of my thesis advance our understanding of the moonlighting function of RbcL in oxidative stress tolerance and the management of oxidized RNA (Dhaliwal, 2021; Zhan *et al.*, 2015).

As is described below, the *rbcL* mutants analyzed here showed either elevated or wild-type oxidative stress tolerance. Previously, elevated stress tolerance of the *RBCS* null mutant (*ΔrbcS*) was hypothesized to involve the remaining non-Rubisco form of RbcL that fractionated to P16-TI (Zhan *et al.*, 2015). Since this elevated stress tolerance phenotype was opposite to the impaired stress tolerance phenotype of the *rbcL* null mutant (*ΔrbcL*), it was presumed to be *required* for oxidative stress tolerance. It should be noted that my results did not show a significant impairment of tolerance in the same *rbcL* null mutant, although the mean tolerance was lower than that of wild type. While the basis of this discrepancy between my results and those found previously is unclear, it may be due to unidentified differences in experimental conditions. The fact that none of the *rbcL* mutants showed *impaired* tolerance might also reflect the existence of a redundant process. The enhanced tolerance phenotypes, however, were significantly different from wild-type tolerance and informative, as described below.

Analyses of mutants that have RbcL in supramolecular states supports a role of the RbcL dimer in the moonlighting function in oxidative stress tolerance (Figure 3). The dimer is distinct from the RbcL supramolecular state that can inhibit its own translation, showing that these moonlighting functions are distinct (Wietrzynski *et al.*, 2021). Interestingly, the P16-TI fraction of both the *ΔrbcS* and *rbcL-L8-mut* exhibited excess RbcL over RbcS in the Triton X-100 insoluble fraction (P16-TI) (Figure 5B, lanes 2 and 5 respectively). This form also was found previously in *ΔrbcS* (Zhan *et al.*, 2015). The *rbcL-L2-mut* also accumulated this insoluble form of RbcL but was

very difficult to detect. It could be that there is a certain threshold that must be met for the moonlighting function of RbcL to come about, and this form is consistently present in the samples, regardless of induced oxidative stress. Lastly, immunofluorescence microscopy shows RbcL punctate bodies in the chloroplast in the mutant strains *ΔrbcS* and *rbcL-L8-mut*. There does not seem to be a distinct location as they appear to be in the lobes, basal region, and translation zone of the chloroplast (Figure 6A). These results are preliminary but suggest that RbcL in punctate bodies may be required for enhanced stress tolerance.

Analyses of four amino acid substitution mutants affecting the RNA-binding domain of RbcL (*rbcL-M42V, rbcL-C53A, rbcL-G54D* and *rbcL-P89R)* provided some evidence of its role in the oxidative stress tolerance. Among these mutants, two showed elevated oxidative stress tolerance relative to wild-type (*rbcL-M42V* and *rbcL-G54D*), whereas tolerance of the other mutants was at the level of wild-type (Figure 4C). While it remains to be determined whether these mutations affect the RNA-binding activity of RbcL, these results provide evidence of roles of residues M42 and G54 in this function. Future work should test for alterations of the RNA-binding activity of these mutant proteins. Interestingly, only the strain carrying *rbcL-G54D* showed an excess level of RbcL in the P16-TI fraction. The strain with *rbcL-M42V* had excess RbcS levels in all three replicate immunoblot trials relative to wild-type (Figure 5B; Supplementary Figure 5B and 5D in Appendix). This was the only variant of the ones tested that exhibited this phenotype suggesting an unknown function of RbcS. Additional work is required to determine the basis of these observations. Furthermore, *rbcL-R217S*, an amino acid substitution mutant that like *rbcL-G54D* is unable to assemble the Rubisco holoenzyme (Thow *et al.*, 1994), accumulated an even greater amount of the insoluble pool than all other mutants. However, this variant demonstrated wild-type levels of stress tolerance (Figure 4D), possibly meaning that if this insoluble pool of

RbcL is too much in excess, it affects stress tolerance. Nevertheless, *rbcL-G54D* showed similar levels to Δ*rbcS* in that this insoluble RbcL pool is present without its assembly partner and demonstrates increased stress tolerance. Additionally, a similar pattern to *rbcL-L8-mut* (described above) was seen in the strain carrying *rbcL-G54D* as there are punctate bodies of RbcL that are present whether there is stress present or not (Figure 6). This could mean that the alternate pool of RbcL needed for stress tolerance and found in the P16-TI fraction is constitutively present in this variant strain. This might be related to its enhanced tolerance to oxidative stress.

Furthermore, the reversible oxidation of certain conserved cysteine residues may be involved in holoenzyme disassembly under oxidizing conditions (García-Murria *et al.*, 2018; Marín-Navarro & Moreno, 2006; Moreno *et al.*, 2008), therefore possibly activating the moonlighting function of RbcL. The cysteine mutants analyzed here were *rbcL-C84S*, *rbcL-C172S, rbcL-C192S/Y226L, rbcL-C247S, rbcL-C284S* and *rbcL-C449S/C459S.* It is important to note that *rbcL-C84S*, *rbcL-C172S* and *rbcL-C449S/C459S* have been investigated previously and the fractions used here were prepared independently (Dhaliwal, 2021). Among the mutants analyzed, only *rbcL-C192S/Y226L, rbcL-C247S* and *rbcL-C284S* showed elevated stress tolerance relative to wild-type (Figure 4C). However, when analyzing their levels of RbcL in the P16-TI fraction, it seemed that only *rbcL-C247S* and possibly *C192S/Y226L* accumulated an excess of RbcL. However, since the signal is extremely low for these samples, it is difficult to come to a conclusion regarding these strains. Little information in the literature is available for some of the mutants listed in this thesis. However, RbcL has been extensively studied in *Chlamydomonas* for its role in Rubisco and, therefore, many mutants have been generated and are available at the stock center.

Future directions for this project could be the creation of a construct to express an affinity purification-tagged RbcL from a mutant (or mutants) with elevated moonlighting functions, such

as *rbcL-G54D* (Appendix I, Supplementary Figure 8). Once this construct is created and transformed into *Chlamydomonas*, it can be subjected to affinity purification and mass spectrometry analysis to identify interacting partners. These results would provide some insight into the binding proteins or complexes that may also be involved alongside RbcL in its moonlighting functions.

References

Afshana, Dar, M. A., & Reshi, Z. A. (2021). Induced Genotoxicity and Oxidative Stress in Plants: An Overview. In Z. Khan, M. Y. K. Ansari, & D. Shahwar (Eds.), *Induced Genotoxicity and Oxidative Stress in Plants* (pp. 1–27). Springer. https://doi.org/10.1007/978-981-16-2074-4_1

Aldred, E. M., Buck, C., & Vall, K. (2009). Chapter 7—Free radicals. In E. M. Aldred, C. Buck, & K. Vall (Eds.), *Pharmacology* (pp. 41–52). Churchill Livingstone. https://doi.org/10.1016/B978-0-443-06898-0.00007-4

Archibald, J. M. (2009). The Puzzle of Plastid Evolution. *Current Biology*, *19*(2), R81–R88. https://doi.org/10.1016/j.cub.2008.11.067

Asada, K. (2000). The Water-Water Cycle as Alternative Photon and Electron Sinks. *Philosophical Transactions: Biological Sciences*, *355*(1402), 1419–1431.

Bakhtiari Koohsorkhi, S. (2021). *The spatial organization of chloroplast protein synthesis and the Calvin Benson Cycle in Chlamydomonas reinhardtii* [PhD, Concordia University]. https://spectrum.library.concordia.ca/id/eprint/990173/

Barone, M. E., Parkes, R., Herbert, H., McDonnell, A., Conlon, T., Aranyos, A., Fierli, D., Fleming, G. T. A., & Touzet, N. (2021). Comparative Response of Marine Microalgae to H2O2-Induced Oxidative Stress. *Applied Biochemistry and Biotechnology*, *193*(12), 4052–4067. https://doi.org/10.1007/s12010-021-03690-x

Bienert, G. P., Schjoerring, J. K., & Jahn, T. P. (2006). Membrane transport of hydrogen peroxide. *Biochimica et Biophysica Acta*, *1758*(8), 994–1003. https://doi.org/10.1016/j.bbamem.2006.02.015

Blaby, I. K., Blaby-Haas, C. E., Pérez-Pérez, M. E., Schmollinger, S., Fitz-Gibbon, S., Lemaire, S. D., & Merchant, S. S. (2015). Genome-wide analysis on *Chlamydomonas reinhardtii* reveals impact of hydrogen peroxide on protein stress responses and overlap with other stress transcriptomes. *The Plant Journal : For Cell and Molecular Biology*, *84*(5), 974–988. https://doi.org/10.1111/tpj.13053

Buchan, J. R., & Parker, R. (2009). Eukaryotic Stress Granules: The Ins and Out of Translation. *Molecular Cell*, *36*(6), 932. https://doi.org/10.1016/j.molcel.2009.11.020

Cao, M., Fu, Y., Guo, Y., & Pan, J. (2009). Chlamydomonas (Chlorophyceae) colony PCR. *Protoplasma*, *235*(1), 107–110. https://doi.org/10.1007/s00709-009-0036-9

Chang, C.-H., Curtis, J. D., Maggi, L. B., Faubert, B., Villarino, A. V., O'Sullivan, D., Huang, S. C.-C., van der Windt, G. J. W., Blagih, J., Qiu, J., Weber, J. D., Pearce, E. J., Jones, R. G., & Pearce, E. L. (2013). Posttranscriptional Control of T Cell Effector Function by Aerobic Glycolysis. *Cell*, *153*(6), 1239–1251. https://doi.org/10.1016/j.cell.2013.05.016

Chatterjee, A. (2013). Reduced Glutathione: A Radioprotector or a Modulator of DNA-Repair Activity? *Nutrients*, *5*(2), 525–542. https://doi.org/10.3390/nu5020525

Chen, Z., & Spreitzer, R. J. (1989). Chloroplast Intragenic Suppression Enhances the Low CO_2/O_2 Specificity of Mutant Ribulose-bisphosphate Carboxylase/Oxygenase. *Journal of Biological Chemistry*, *264*(6), 3051–3053. https://doi.org/10.1016/S0021-9258(18)94027-5

Chen, Z., Yu, W., Lee, J. H., Diao, R., & Spreitzer, R. J. (1991). Complementing amino acid substitutions within loop 6 of the alpha/beta-barrel active site influence the carbon dioxide/oxygen specificity of chloroplast ribulose-1,5-bisphosphate

carboxylase/oxygenase. *Biochemistry*, *30*(36), 8846–8850. https://doi.org/10.1021/bi00100a017

Das, K., & Roychoudhury, A. (2014). Reactive oxygen species (ROS) and response of antioxidants as ROS-scavengers during environmental stress in plants. *Frontiers in Environmental Science*, *2*. https://www.frontiersin.org/articles/10.3389/fenvs.2014.00053

Davies, M. J., Fu, S., Wang, H., & Dean, R. T. (1999). Stable markers of oxidant damage to proteins and their application in the study of human disease. *Free Radical Biology and Medicine*, *27*(11), 1151–1163. https://doi.org/10.1016/S0891-5849(99)00206-3

Dent, R. M., Haglund, C. M., Chin, B. L., Kobayashi, M. C., & Niyogi, K. K. (2005). Functional Genomics of Eukaryotic Photosynthesis Using Insertional Mutagenesis of *Chlamydomonas reinhardtii. Plant Physiology*, *137*(2), 545–556. https://doi.org/10.1104/pp.104.055244

Dhaliwal, J. S. (2021). *Quality Control of Oxidized RNA in Saccharomyces cerevisiae and Chlamydomonas reinhardtii* [PhD, Concordia University]. https://spectrum.library.concordia.ca/id/eprint/989981/

Dhaliwal, J. S., Panozzo, C., Benard, L., & Zerges, W. (2022). An RNA granule for translation quality control in *Saccharomyces cerevisiae*. *Journal of Cell Science*, *135*(23), jcs260388. https://doi.org/10.1242/jcs.260388

Du, Y.-C., Peddi, S. R., & Spreitzer, R. J. (2003). Assessment of Structural and Functional Divergence Far from the Large Subunit Active Site of Ribulose-1,5-bisphosphate Carboxylase/Oxygenase*. *Journal of Biological Chemistry*, *278*(49), 49401–49405. https://doi.org/10.1074/jbc.M309993200

Du, Y.-C., & Spreitzer, R. J. (2000). Suppressor Mutations in the Chloroplast-encoded Large Subunit Improve the Thermal Stability of Wild-type Ribulose-1,5-bisphosphate Carboxylase/Oxygenase*. *Journal of Biological Chemistry*, *275*(26), 19844–19847. https://doi.org/10.1074/jbc.M002321200

Esquível, M. G., Pinto, T. S., Marín-Navarro, J., & Moreno, J. (2006). Substitution of tyrosine residues at the aromatic cluster around the betaA-betaB loop of rubisco small subunit affects the structural stability of the enzyme and the *in vivo* degradation under stress conditions. *Biochemistry*, *45*(18), 5745–5753. https://doi.org/10.1021/bi052588y

Foyer, C. H., & Noctor, G. (2005). Redox Homeostasis and Antioxidant Signaling: A Metabolic Interface between Stress Perception and Physiological Responses. *The Plant Cell*, *17*(7), 1866–1875. https://doi.org/10.1105/tpc.105.033589

Foyer, C. H., & Noctor, G. (2009). Redox Regulation in Photosynthetic Organisms: Signaling, Acclimation, and Practical Implications. *Antioxidants & Redox Signaling*, *11*(4), 861–905. https://doi.org/10.1089/ars.2008.2177

Foyer, C. H., & Shigeoka, S. (2011). Understanding Oxidative Stress and Antioxidant Functions to Enhance Photosynthesis1. *Plant Physiology*, *155*(1), 93–100. https://doi.org/10.1104/pp.110.166181

Freeman Rosenzweig, E. S., Xu, B., Kuhn Cuellar, L., Martinez-Sanchez, A., Schaffer, M., Strauss, M., Cartwright, H. N., Ronceray, P., Plitzko, J. M., Förster, F., Wingreen, N. S., Engel, B. D., Mackinder, L. C. M., & Jonikas, M. C. (2017). The Eukaryotic CO_2-Concentrating Organelle Is Liquid-like and Exhibits Dynamic Reorganization. *Cell*, *171*(1), 148-162.e19. https://doi.org/10.1016/j.cell.2017.08.008

García-Murria, M. J., Sudhani, H. P. K., Marín-Navarro, J., Sánchez del Pino, M. M., & Moreno, J. (2018). Dissecting the individual contribution of conserved cysteines to the redox regulation of RubisCO. *Photosynthesis Research*, *137*(2), 251–262. https://doi.org/10.1007/s11120-018-0497-9

Garcin, E. D. (2019). GAPDH as a model non-canonical AU-rich RNA binding protein. *Seminars in Cell & Developmental Biology*, *86*, 162–173. https://doi.org/10.1016/j.semcdb.2018.03.013

Gill, S. S., & Tuteja, N. (2010). Reactive oxygen species and antioxidant machinery in abiotic stress tolerance in crop plants. *Plant Physiology and Biochemistry*, *48*(12), 909–930. https://doi.org/10.1016/j.plaphy.2010.08.016

Green, M. R., & Sambrook, J. (2018). Touchdown Polymerase Chain Reaction (PCR). *Cold Spring Harbor Protocols*, *2018*(5). https://doi.org/10.1101/pdb.prot095133

Harris, E. H. (1989). The Chlamydomonas Sourcebook. In *The Chlamydomonas Sourcebook. A Comprehensive Guide to Biology and Laboratory Use.* (246th ed., pp. 25–63). Academic Press. https://doi.org/10.1016/B978-0-12-326880-8.50007-9

Harris, E. H. (2001). Chlamydomonas as a Model Organism. *Annual Review of Plant Physiology and Plant Molecular Biology*, *52*(1), 363–406. https://doi.org/10.1146/annurev.arplant.52.1.363

Hu, Z., Cools, T., & De Veylder, L. (2016). Mechanisms Used by Plants to Cope with DNA Damage. *Annual Review of Plant Biology*, *67*(1), 439–462. https://doi.org/10.1146/annurev-arplant-043015-111902

Jiang, X., & Stern, D. (2009). Mating and Tetrad Separation of *Chlamydomonas reinhardtii* for Genetic Analysis. *Journal of Visualized Experiments : JoVE*, *30*, 1274. https://doi.org/10.3791/1274

Johnson, X. (2011). Manipulating RuBisCO accumulation in the green alga, *Chlamydomonas reinhardtii*. *Plant Molecular Biology*, *76*(3), 397–405. https://doi.org/10.1007/s11103-011-9783-z

Kedersha, N. L., Gupta, M., Li, W., Miller, I., & Anderson, P. (1999). RNA-Binding Proteins Tia-1 and Tiar Link the Phosphorylation of Eif-2α to the Assembly of Mammalian Stress Granules. *The Journal of Cell Biology*, *147*(7), 1431–1442.

Kim, H.-Y. (2013). The Methionine Sulfoxide Reduction System: Selenium Utilization and Methionine Sulfoxide Reductase Enzymes and Their Functions. *Antioxidants & Redox Signaling*, *19*(9), 958–969. https://doi.org/10.1089/ars.2012.5081

Kim, K.-S., Feild, E., King, N., Yaoi, T., Kustu, S., & Inwood, W. (2005). Spontaneous Mutations in the Ammonium Transport Gene AMT4 of *Chlamydomonas reinhardtii. Genetics*, *170*(2), 631–644. https://doi.org/10.1534/genetics.105.041574

Knight, S., Andersson, I., & Brändén, C.-I. (1990). Crystallographic analysis of ribulose 1,5-bisphosphate carboxylase from spinach at 2·4 Å resolution: Subunit interactions and active site. *Journal of Molecular Biology*, *215*(1), 113–160. https://doi.org/10.1016/S0022-2836(05)80100-7

Knopf, J. A., & Shapira, M. (2005). Degradation of Rubisco SSU during oxidative stress triggers aggregation of Rubisco particles in *Chlamydomonas reinhardtii. Planta*, *222*(5), 787–793. https://doi.org/10.1007/s00425-005-0023-0

Larson, E. M., O'Brien, C. M., Zhu, G., Spreitzer, R. J., & Portis, A. R. (1997). Specificity for Activase Is Changed by a Pro-89 to Arg Substitution in the Large Subunit of Ribulose-1,5-bisphosphate Carboxylase/Oxygenase. *Journal of Biological Chemistry*, *272*(27), 17033–17037. https://doi.org/10.1074/jbc.272.27.17033

Li, Z., Wu, J., & DeLeo, C. J. (2006). RNA damage and surveillance under oxidative stress. *IUBMB Life*, *58*(10), 581–588. https://doi.org/10.1080/15216540600946456

Liu, H., & Jeffery, C. J. (2020). Moonlighting Proteins in the Fuzzy Logic of Cellular Metabolism. *Molecules*, *25*(15), 3440. https://doi.org/10.3390/molecules25153440

Liu, Z., Chen, X., Li, Z., Ye, W., Ding, H., Li, P., & Aung, L. H. H. (2020). Role of RNA Oxidation in Neurodegenerative Diseases. *International Journal of Molecular Sciences*, *21*(14), 5022. https://doi.org/10.3390/ijms21145022

Mackinder, L. C. M., Meyer, M. T., Mettler-Altmann, T., Chen, V. K., Mitchell, M. C., Caspari, O., Freeman Rosenzweig, E. S., Pallesen, L., Reeves, G., Itakura, A., Roth, R., Sommer, F., Geimer, S., Mühlhaus, T., Schroda, M., Goodenough, U., Stitt, M., Griffiths, H., & Jonikas, M. C. (2016). A repeat protein links Rubisco to form the eukaryotic carbon-concentrating organelle. *Proceedings of the National Academy of Sciences*, *113*(21), 5958–5963. https://doi.org/10.1073/pnas.1522866113

Marín-Navarro, J., & Moreno, J. (2006). Cysteines 449 and 459 modulate the reduction–oxidation conformational changes of ribulose 1·5-bisphosphate carboxylase/oxygenase and the translocation of the enzyme to membranes during stress. *Plant, Cell & Environment*, *29*(5), 898–908. https://doi.org/10.1111/j.1365-3040.2005.01469.x

Mazroui, R., Sukarieh, R., Bordeleau, M.-E., Kaufman, R. J., Northcote, P., Tanaka, J., Gallouzi, I., & Pelletier, J. (2006). Inhibition of Ribosome Recruitment Induces Stress Granule

Formation Independently of Eukaryotic Initiation Factor 2α Phosphorylation. *Molecular Biology of the Cell*, *17*(10), 4212–4219. https://doi.org/10.1091/mbc.E06-04-0318

McDonagh, B. (2017). Detection of ROS Induced Proteomic Signatures by Mass Spectrometry. *Frontiers in Physiology*, *8*. https://www.frontiersin.org/articles/10.3389/fphys.2017.00470

Moreno, J., García-Murria, M. J., & Marín-Navarro, J. (2008). Redox modulation of Rubisco conformation and activity through its cysteine residues. *Journal of Experimental Botany*, *59*(7), 1605–1614. https://doi.org/10.1093/jxb/erm310

Nandi, A., Yan, L.-J., Jana, C. K., & Das, N. (2019). Role of Catalase in Oxidative Stress- and Age-Associated Degenerative Diseases. *Oxidative Medicine and Cellular Longevity*, *2019*, 9613090. https://doi.org/10.1155/2019/9613090

Nickelsen, J., & Kück, U. (2000). The Unicellular Green Alga *Chlamydomonas reinhardtii* as an Experimental System to Study Chloroplast RNA Metabolism. *Naturwissenschaften*, *87*(3), 97–107. https://doi.org/10.1007/s001140050686

Nozaki, H., Onishi, K., & Morita, E. (2002). Differences in Pyrenoid Morphology Are Correlated with Differences in the rbcL Genes of Members of the Chloromonas Lineage (Volvocales, Chlorophyceae). *Journal of Molecular Evolution*, *55*(4), 414–430. https://doi.org/10.1007/s00239-002-2338-9

Nunomura, A., Hofer, T., Moreira, P. I., Castellani, R. J., Smith, M. A., & Perry, G. (2009). RNA oxidation in Alzheimer disease and related neurodegenerative disorders. *Acta Neuropathologica*, *118*(1), 151–166. https://doi.org/10.1007/s00401-009-0508-1

Pröschold, T., Harris, E. H., & Coleman, A. W. (2005). Portrait of a Species: *Chlamydomonas reinhardtii. Genetics*, *170*(4), 1601–1610. https://doi.org/10.1534/genetics.105.044503

Randolph-Anderson, B. L., Gillham, N. W., & Boynton, J. E. (1989). Electrophoretic and immunological comparisons of chloroplast and prokaryotic ribosomal proteins reveal that certain families of large subunit proteins are evolutionarily conserved. *Journal of Molecular Evolution*, *29*(1), 68–88. https://doi.org/10.1007/BF02106183

Ray, P. D., Huang, B.-W., & Tsuji, Y. (2012). Reactive oxygen species (ROS) homeostasis and redox regulation in cellular signaling. *Cellular Signalling*, *24*(5), 981–990. https://doi.org/10.1016/j.cellsig.2012.01.008

Sambrook, J., & Russell, D. W. (2001a). Preparation of Buffers and Stock Solutions. In *Molecular Cloning—A Laboratory Manual* (Third, Vol. 3, p. A8.43). Cold Spring Harbor Laboratory Press.

Sambrook, J., & Russell, D. W. (2001b). SDS-Polyacrylamide Gel Electrophoresis of Proteins. In *Molecular Cloning—A Laboratory Manual* (Third, Vol. 3, p. A8.43). Cold Spring Harbor Laboratory Press.

Santos-Sánchez, N. F., Salas-Coronado, R., Villanueva-Cañongo, C., Hernández-Carlos, B., Santos-Sánchez, N. F., Salas-Coronado, R., Villanueva-Cañongo, C., & Hernández-Carlos, B. (2019). Antioxidant Compounds and Their Antioxidant Mechanism. *Antioxidants*. IntechOpen. https://doi.org/10.5772/intechopen.85270

Sasso, S., Stibor, H., Mittag, M., & Grossman, A. R. (2018). From molecular manipulation of domesticated *Chlamydomonas reinhardtii* to survival in nature. *ELife*, *7*, e39233. https://doi.org/10.7554/eLife.39233

Satagopan, S., & Spreitzer, R. J. (2004). Substitutions at the Asp-473 Latch Residue of Chlamydomonas Ribulosebisphosphate Carboxylase/Oxygenase Cause Decreases in

Carboxylation Efficiency and CO_2/O_2 Specificity. *Journal of Biological Chemistry*, *279*(14), 14240–14244. https://doi.org/10.1074/jbc.M313215200

Simms, C. L., Hudson, B. H., Mosior, J. W., Rangwala, A. S., & Zaher, H. S. (2014). An active role for the ribosome in determining the fate of oxidized mRNA. *Cell Reports*, *9*(4), 1256–1264. https://doi.org/10.1016/j.celrep.2014.10.042

Spreitzer, R. J. (1993). Genetic Dissection of Rubisco Structure and Function. *Annual Review of Plant Physiology and Plant Molecular Biology*, *44*, 411–434.

Spreitzer, R. J., Al-Abed, S. R., & Huether, M. J. (1988). Temperature-Sensitive, Photosynthesis-Deficient Mutants of *Chlamydomonas reinhardtii*. *Plant Physiology*, *86*(3), 773–777. https://doi.org/10.1104/pp.86.3.773

Spreitzer, R. J., & Mets, L. (1981). Photosynthesis-deficient Mutants of *Chlamydomonas reinhardii* with Associated Light-sensitive Phenotypes 1. *Plant Physiology*, *67*(3), 565–569. https://doi.org/10.1104/pp.67.3.565

Spreitzer, R. J., & Ogren, W. L. (1983). Rapid recovery of chloroplast mutations affecting ribulosebisphosphate carboxylase/oxygenase in *Chlamydomonas reinhardtii*. *Proceedings of the National Academy of Sciences*, *80*(20), 6293–6297. https://doi.org/10.1073/pnas.80.20.6293

Spreitzer, R. J., & Salvucci, M. E. (2002). RUBISCO: Structure, Regulatory Interactions, and Possibilities for a Better Enzyme. *Annual Review of Plant Biology*, *53*(1), 449–475. https://doi.org/10.1146/annurev.arplant.53.100301.135233

Spreitzer, R. J., Thow, G., & Zhu, G. (1995). Pseudoreversion Substitution at Large-Subunit Residue 54 Influences the CO_2/O_2 Specificity of Chloroplast Ribulose-Bisphosphate

Carboxylase/Oxygenase. *Plant Physiology*, *109*(2), 681–685. https://doi.org/10.1104/pp.109.2.681

Strober, W. (2015). Trypan Blue Exclusion Test of Cell Viability. *Current Protocols in Immunology*, *111*, A3.B.1-A3.B.3. https://doi.org/10.1002/0471142735.ima03bs111

Thow, G., Zhu, G., & Spreitzer, R. J. (1994). Complementing Substitutions within Loop Regions 2 and 3 of the alpha/beta-Barrel Active Site Influence the CO_2/O_2 Specificity of Chloroplast Ribulose-1,5-bisphosphate Carboxylase/Oxygenase. *Biochemistry*, *33*(17), 5109–5114. https://doi.org/10.1021/bi00183a014

Tsanov, N., Samacoits, A., Chouaib, R., Traboulsi, A.-M., Gostan, T., Weber, C., Zimmer, C., Zibara, K., Walter, T., Peter, M., Bertrand, E., & Mueller, F. (2016). SmiFISH and FISH-quant – a flexible single RNA detection approach with super-resolution capability. *Nucleic Acids Research*, *44*(22), e165. https://doi.org/10.1093/nar/gkw784

Uniacke, J., Colón-Ramos, D., & Zerges, W. (2011). FISH and Immunofluorescence Staining in Chlamydomonas. In J. E. Gerst (Ed.), *RNA Detection and Visualization: Methods and Protocols* (pp. 15–29). Humana Press. https://doi.org/10.1007/978-1-61779-005-8_2

Uniacke, J., & Zerges, W. (2008). Stress induces the assembly of RNA granules in the chloroplast of *Chlamydomonas reinhardtii. The Journal of Cell Biology*, *182*(4), 641–646. https://doi.org/10.1083/jcb.200805125

Uniacke, J., & Zerges, W. (2009). Chloroplast protein targeting involves localized translation in Chlamydomonas. *Proceedings of the National Academy of Sciences of the United States of America*, *106*(5), 1439–1444. https://doi.org/10.1073/pnas.0811268106

Wefers, Z., Alecki, C., Huang, R., Jacob-Tomas, S., & Vera, M. (2022). Analysis of the Expression and Subcellular Distribution of eEF1A1 and eEF1A2 mRNAs during Neurodevelopment. *Cells*, *11*(12), Article 12. https://doi.org/10.3390/cells11121877

Wietrzynski, W., Traverso, E., Wollman, F.-A., & Wostrikoff, K. (2021). The state of oligomerization of Rubisco controls the rate of synthesis of the Rubisco large subunit in *Chlamydomonas reinhardtii*. *The Plant Cell*, *33*(5), 1706–1727. https://doi.org/10.1093/plcell/koab061

Winterbourn, C. C. (2013). Chapter One—The Biological Chemistry of Hydrogen Peroxide. In E. Cadenas & L. Packer (Eds.), *Methods in Enzymology* (Vol. 528, pp. 3–25). Academic Press. https://doi.org/10.1016/B978-0-12-405881-1.00001-X

Wurtmann, E. J., & Wolin, S. L. (2009). RNA under attack: Cellular handling of RNA damage. *Critical Reviews in Biochemistry and Molecular Biology*, *44*(1), 34–49. https://doi.org/10.1080/10409230802594043

Yosef, I., Irihimovitch, V., Knopf, J. A., Cohen, I., Orr-Dahan, I., Nahum, E., Keasar, C., & Shapira, M. (2004). RNA Binding Activity of the Ribulose-1,5-bisphosphate Carboxylase/Oxygenase Large Subunit from *Chlamydomonas reinhardtii*. *Journal of Biological Chemistry*, *279*(11), 10148–10156. https://doi.org/10.1074/jbc.M308602200

Zamora, I., Feldman, J. L., & Marshall, W. F. (2004). PCR-based assay for mating type and diploidy in Chlamydomonas. *BioTechniques*, *37*(4), 534–536. https://doi.org/10.2144/04374BM01

Zhan, Y., Dhaliwal, J. S., Adjibade, P., Uniacke, J., Mazroui, R., & Zerges, W. (2015). Localized control of oxidized RNA. *Journal of Cell Science*, *128*(22), 4210–4219. https://doi.org/10.1242/jcs.175232

Zhan, Y., Marchand, C. H., Maes, A., Mauries, A., Sun, Y., Dhaliwal, J. S., Uniacke, J., Arragain, S., Jiang, H., Gold, N. D., Martin, V. J. J., Lemaire, S. D., & Zerges, W. (2018). Pyrenoid functions revealed by proteomics in *Chlamydomonas reinhardtii*. *PLoS ONE*, *13*(2). https://doi.org/10.1371/journal.pone.0185039

Zhu, G., Kurek, I., & Liu, L. (2010). Chapter 20 Engineering Photosynthetic Enzymes Involved in CO2–Assimilation by Gene Shuffling. In C. A. Rebeiz, C. Benning, H. J. Bohnert, H. Daniell, J. K. Hoober, H. K. Lichtenthaler, A. R. Portis, & B. C. Tripathy (Eds.), *The Chloroplast: Basics and Applications* (pp. 307–322). Springer Netherlands. https://doi.org/10.1007/978-90-481-8531-3_20

Appendix I

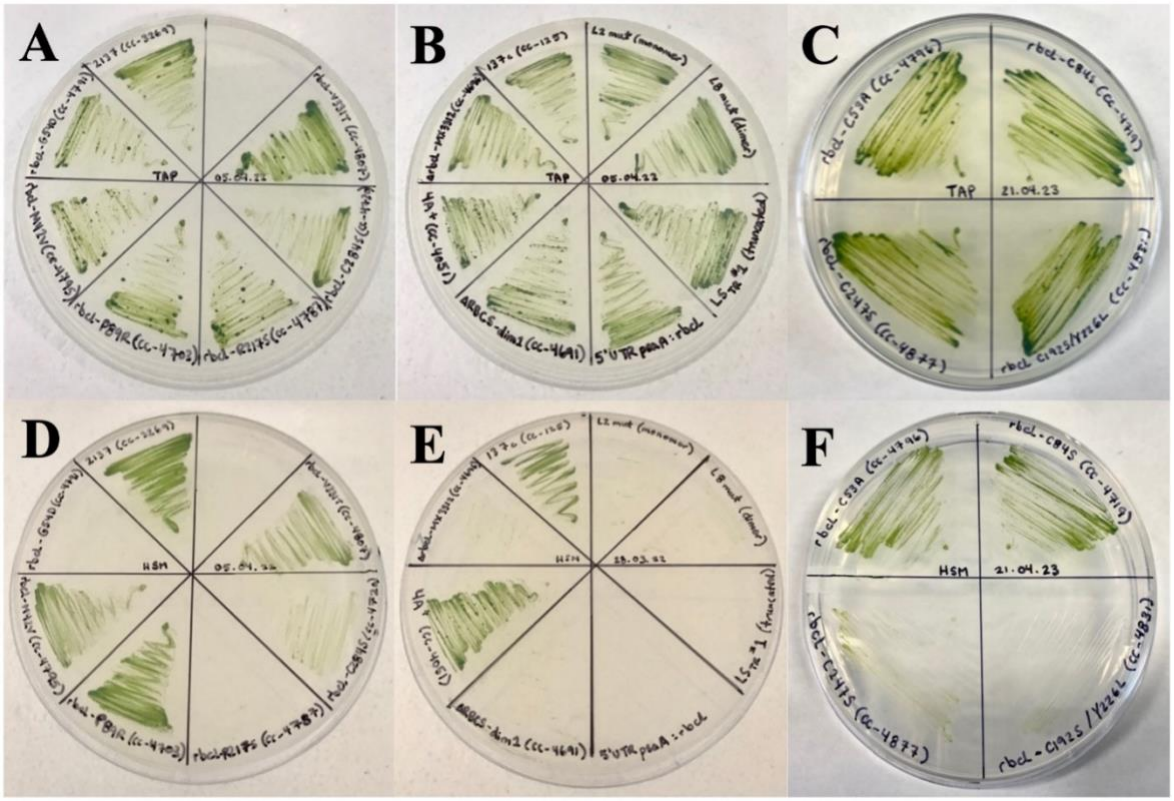

Supplementary Figure 1. Photoautotrophic growth of site-directed mutants and supramolecular state mutants. (A, D) Wild-type strain 2137 as well as strains carrying *rbcL-M42V, rbcL-G54D, rbcL-P89R, rbcL-R217S, rbcL-C284S* and *rbcL-V331T* were streaked on agar plates containing (A) TAP medium (supplemented carbon source) grown in the dark or (D) HSM medium (no carbon source) grown in the light. (B, E) Wild-type strains 4A+ and 137c as well as provided strains carrying RbcL supramolecular states (Δ*rbcL,* Δ*rbcS, rbcL-L2-mut*, *rbcL-L8-mut*, 5'UTR *psaA:rbcL,* LStr) were streaked on agar plates containing (B) TAP medium grown in the dark or (E) HSM medium grown in the light. (C, F) Strains carrying *rbcL-C53A, rbcL-C84S, rbcL-C247S* and *rbcL-C192S/Y226L* were streaked on agar plates containing (C) TAP medium grown in the dark or (F) HSM medium grown in the light. (D-F) Mutants that did not grow on HSM medium imply they do not have Rubisco and are not photoautotrophic.

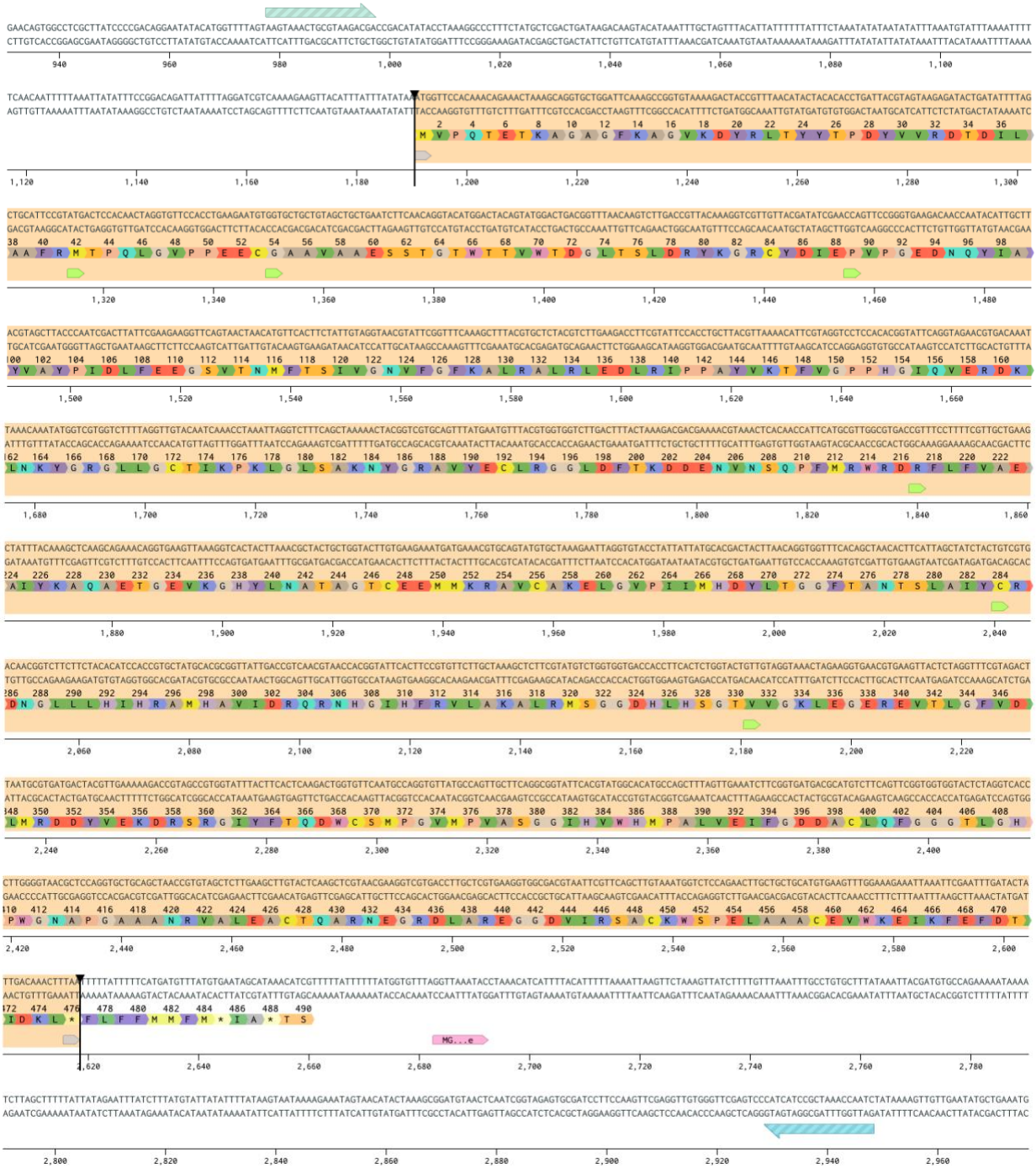

Supplementary Figure 2. Designing oligonucleotides using Benchling to isolate the *rbcL* allele in each mutant strain. The section highlighted in orange corresponds to the RbcL sequence (accession number J01399). The light green arrow upstream of the RbcL sequence is the forward oligonucleotide, whereas the blue arrow downstream is the reverse oligonucleotide.

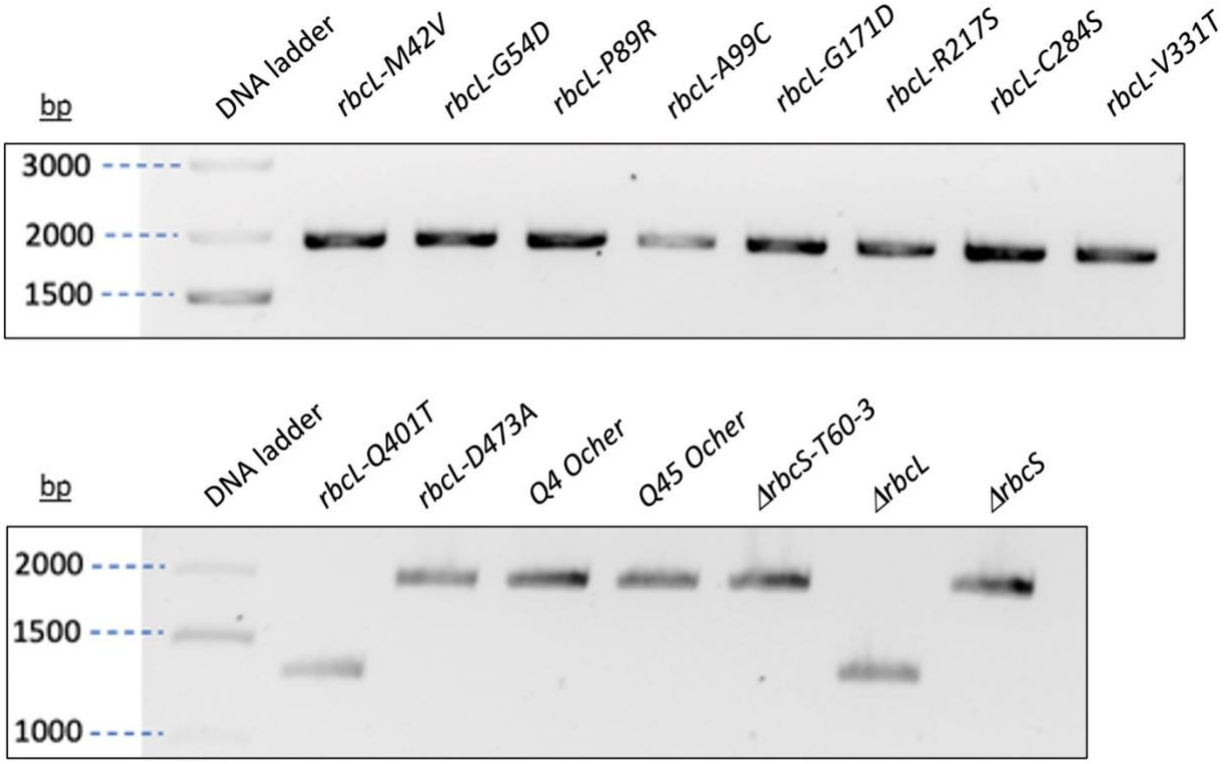

Supplementary Figure 3. PCR verification for the presence of the correct *rbcL* allele in each mutant strain. DNA template obtained from colony PCR of each mutant was used to obtain the associated amplicon of interest. The DNA ladder used here was GeneRuler 1 kb Plus DNA ladder (SM1331, ThermoScientific). Strains that do not have the *rbcL* gene resulted in amplicons of 1400 base pairs (bp), whereas those that do yield amplicons of 1900 bp. Some mutants shown here were not used in this thesis as: 1) they did not contain the correct size amplicon (*i.e.*, *rbcL-Q401T*) or 2) after DNA sequencing, lacked the correct amino acid residue substitution (*i.e.*, *rbcL-A99C, rbcL-G171D, rbcL-D473A,* Q4 Ocher and Q45 Ocher).

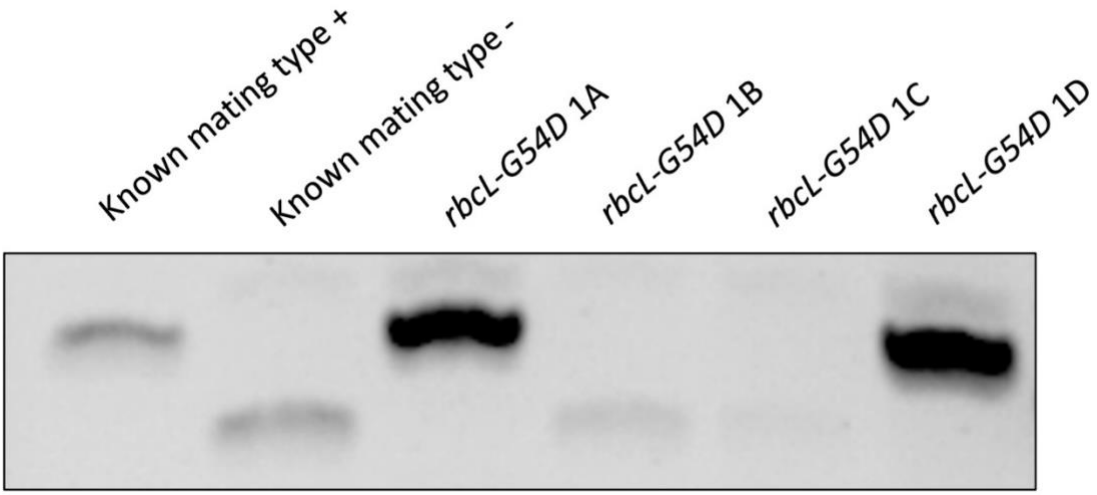

Supplementary Figure 4. Confirming mating type for backcrosses of strain carrying *rbcL-G54D*. Colony PCR was used to obtain the template DNA of known mating type strains as well as the progeny after tetrad dissection. The known mating type plus (+) amplicon resulted in a band of about 700 base pairs (bp), whereas the known mating type minus (-) yielded a 600 bp band. Progeny *rbcL-G54D* 1A and 1D were therefore of mating type (+) and were backcrossed to wild-type once more to clean up any background modifiers.

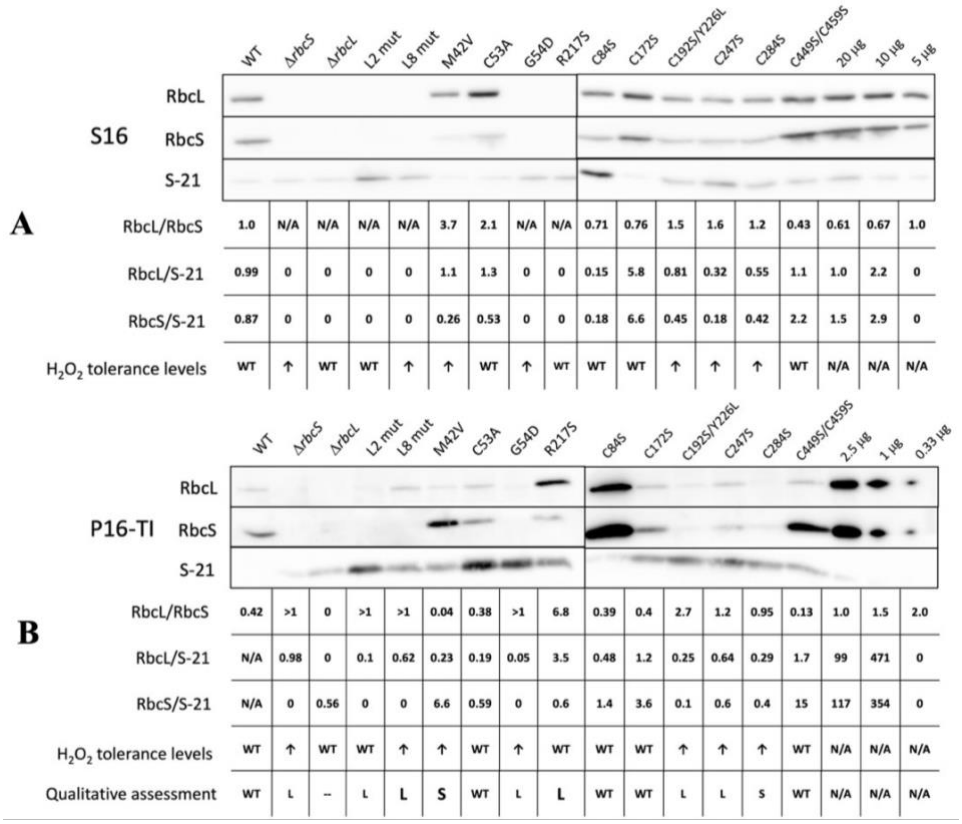
WT
ΔrbcS
ΔrbcL
L2 mut
L8 mut
M42V
C53A
G54D
R217S
C84S
C172S
C192S/Y226L
C247S
C284S
C449S/C459S
20 µg
10 µg
5 µg
RbcL
S16
RbcS
S-21
A
RbcL/RbcS 1.0 N/A N/A N/A N/A 3.7 2.1 N/A N/A 0.71 0.76 1.5 1.6 1.2 0.43 0.61 0.67 1.0
RbcL/S-21 0.99 0 0 0 0 1.1 1.3 0 0 0.15 5.8 0.81 0.32 0.55 1.1 1.0 2.2 0
RbcS/S-21 0.87 0 0 0 0 0.26 0.53 0 0 0.18 6.6 0.45 0.18 0.42 2.2 1.5 2.9 0
H2O2 tolerance levels WT ↑ WT WT ↑ ↑ WT ↑ WT WT WT ↑ ↑ ↑ WT N/A N/A N/A
WT
ΔrbcS
ΔrbcL
L2 mut
L8 mut
M42V
C53A
G54D
R217S
C84S
C172S
C192S/Y226L
C247S
C284S
C449S/C459S
2.5 µg
1 µg
0.33 µg
RbcL
P16-TI
RbcS
S-21
B
RbcL/RbcS 0.42 >1 0 >1 >1 0.04 0.38 >1 6.8 0.39 0.4 2.7 1.2 0.95 0.13 1.0 1.5 2.0
RbcL/S-21 N/A 0.98 0 0.1 0.62 0.23 0.19 0.05 3.5 0.48 1.2 0.25 0.64 0.29 1.7 99 471 0
RbcS/S-21 N/A 0 0.56 0 0 6.6 0.59 0 0.6 1.4 3.6 0.1 0.6 0.4 15 117 354 0
H2O2 tolerance levels WT ↑ WT WT ↑ ↑ WT ↑ WT WT WT ↑ ↑ ↑ WT N/A N/A N/A
Qualitative assessment WT L – L L S WT L L WT WT L L S WT N/A N/A N/A
WT
ΔrbcS
ΔrbcL
L2 mut
L8 mut
M42V
C53A
G54D
R217S
C84S
C172S
C192S/Y226L
C247S
C284S
C449S/C459S
20 µg
10 µg
5 µg
RbcL
S16
RbcS
S-21
C
RbcL/RbcS 1.0 N/A N/A N/A N/A 1.5 1.6 N/A N/A N/A N/A 1.5 1.1 N/A N/A N/A 1.2 1.5
RbcL/S-21 1.5 0 0 0 0 0.11 0.14 0 0 2.1 1.8 0.35 0.3 0.4 N/A 2.5 3.1 0
RbcS/S-21 4.0 0 0 0 0 0.19 0.23 0 0 N/A N/A 0.64 0.74 N/A N/A N/A 7.0 0
H2O2 tolerance levels WT ↑ WT WT ↑ ↑ WT ↑ WT WT WT ↑ ↑ ↑ WT N/A N/A N/A
WT
ΔrbcS
ΔrbcL
L2 mut
L8 mut
M42V
C53A
G54D
R217S
C84S
C172S
C192S/Y226L
C247S
C284S
C449S/C459S
2.5 µg
1 µg
0.33 µg
RbcL
P16-TI
RbcS
S-21
D
RbcL/RbcS 0.31 >1 0 >1 >1 0.12 0.80 >1 25 0.44 0.77 1.8 2.2 0.21 0.1 1.1 0.85 1
RbcL/S-21 2.9 1.6 0 0.26 1.9 2.5 0.95 3.7 22 7.1 8.0 2.6 5.0 0 7.7 678 1604 0
RbcS/S-21 22 0 0 0 0 47 2.8 0 2.0 38 25 3.3 5.3 27 179 1475 4448 0
H2O2 tolerance levels WT ↑ WT WT ↑ ↑ WT ↑ WT WT WT ↑ ↑ ↑ WT N/A N/A N/A
Qualitative assessment WT L – L L S WT L L WT WT L L WT WT N/A N/A N/A

Supplementary Figure 5. Replicate immunoblot trials to ascertain the levels of wild-type and mutant RbcL in soluble and Triton-insoluble forms. (A-D) Replicate trials of the supernatant fraction (S16) and the Triton X-100 insoluble pellet fraction (P16-TI) of wild-type and mutant cell lysates were analyzed by SDS-PAGE and immunoblot analyses. The blots were incubated with antisera raised against RbcL, RbcS and the chloroplast ribosomal protein S-21 as a control for the amount of protein in each lane. A dilution series of the wild-type S16 extract was included on each blot to reveal proportionality of signal to RbcL. Black vertical lines in (A-D) indicate joining of blots which were performed and imaged entirely in parallel (*i.e.*, under identical conditions and ECL imager settings and exposures). Blots from (A) and (C) were from shorter exposure than the blots from (B) and (D) due to the higher concentration of S16 proteins than in the P16-TI fractions. Below each blot is a quantification table of the RbcL to RbcS ratio (RbcL/RbcS), the RbcL to S-21 ratio (RbcL/S-21) and RbcS to S-21 ratio (RbcS/S-21). A '>1' indicates an excess of RbcL relative to in wild-type. The oxidative stress tolerance (H_2O_2) for wild-type and the mutants was also indicated as follows: an upwards arrow (↑) refers to enhanced stress tolerance, and 'WT' refers to wild-type levels of stress tolerance. 'L' and 'S' refer to excess RbcL and RbcS, respectively, compared to in wild-type, whereas '--' indicated non-detection and 'WT' indicated a wild-type RbcL to RbcS ratio. The font size of the letters indicates the degree of the difference from wild-type.

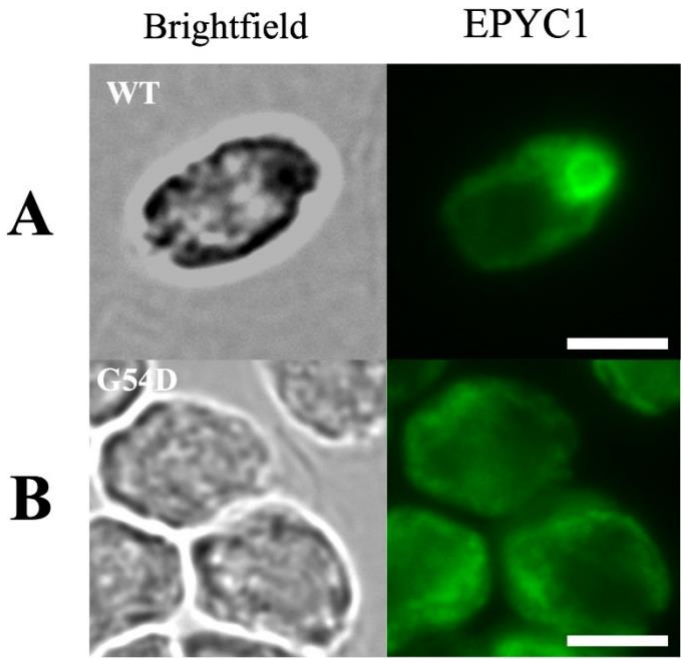

Supplementary Figure 6. Control for pyrenoid formation in the strain carrying *rbcL-G54D*. (A) Wild-type strain 2137 is shown in the brightfield channel alongside immunofluorescence staining with EPYC1, a pyrenoid marker (in green), at a dilution of 1:1000. (B) The strain carrying *rbcL-G54D* is shown in the brightfield channel alongside immunofluorescence staining with EPYC1 (in green). Scale bars indicate 5 μm in length.

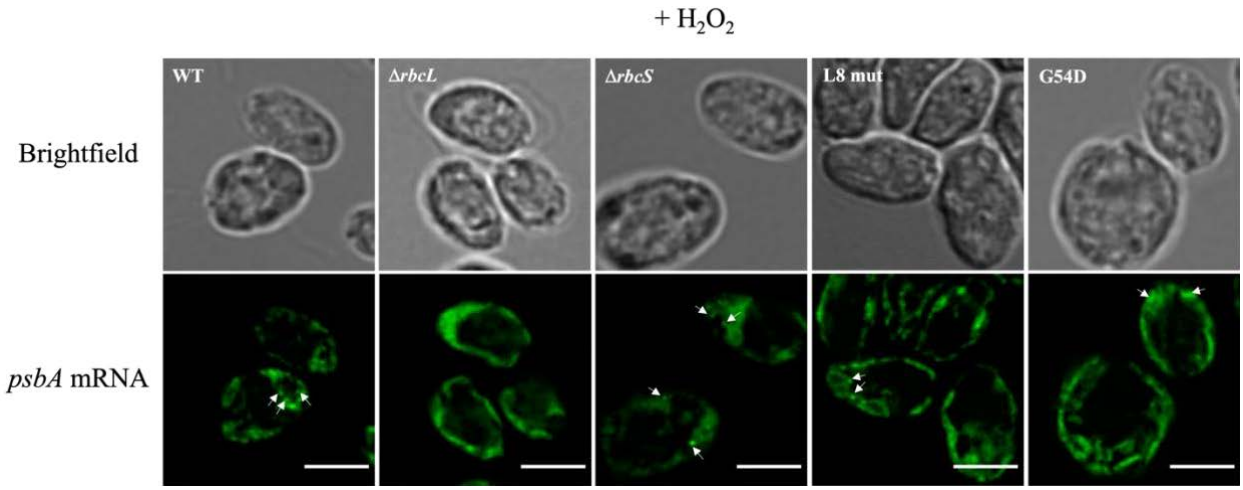

Supplementary Figure 7. Fluorescence *in situ* hybridization (FISH) of a chloroplast stress granule marker in site-directed and supramolecular state mutants. All strains were subjected to 2 mM H_2O_2 for 1 hour. Wild-type alongside strains carrying Δ*rbcL,* Δ*rbcS, rbcL-L8-mut* and *rbcL-G54D* were imaged in brightfield as well as in the Texas-Red channel with *psbA* mRNA (shown in green), a chloroplast stress granule marker. White arrows show the possible formation of chloroplast stress granules. Scale bars indicate 5 μm in length.

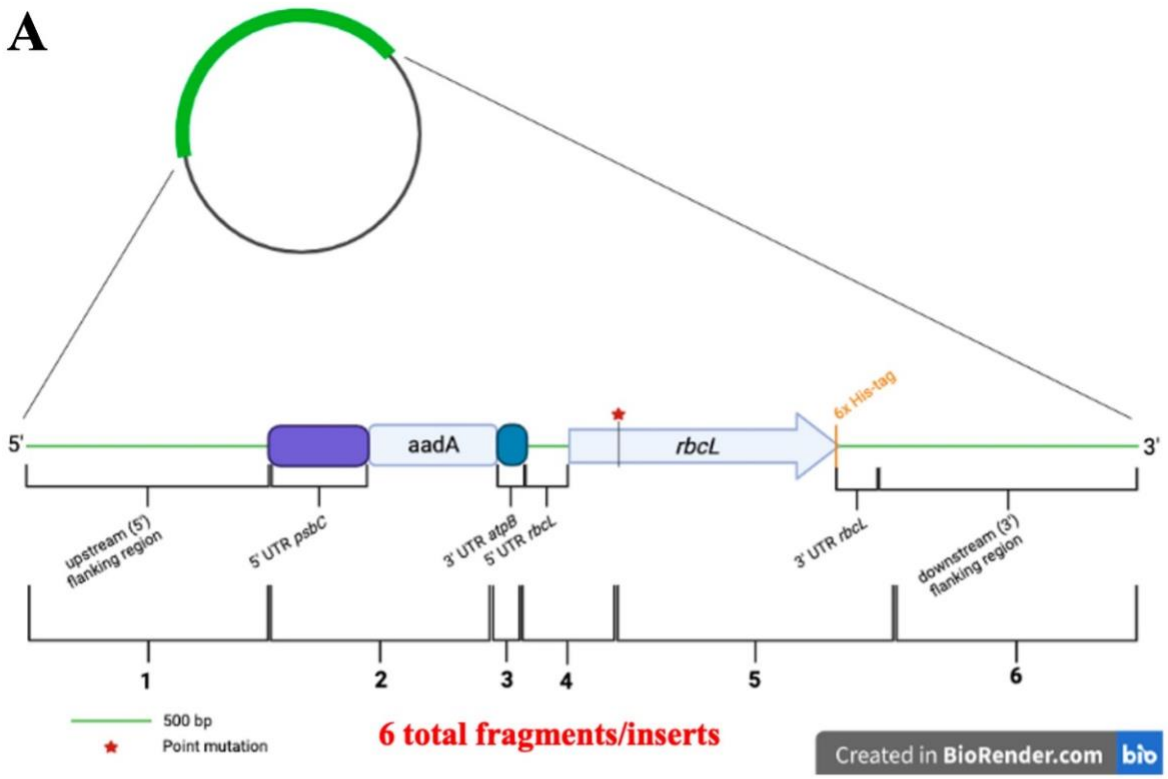
A
5'
aadA
rbcL
6x His-tag
3'
upstream (5') flanking region
5'UTR psbC
3'UTR atpB
5'UTR rbcL
3'UTR rbcL
downstream (3') flanking region
1
2
3
4
5
6
500 bp
Point mutation
6 total fragments/inserts
Created in BioRender.com
bio

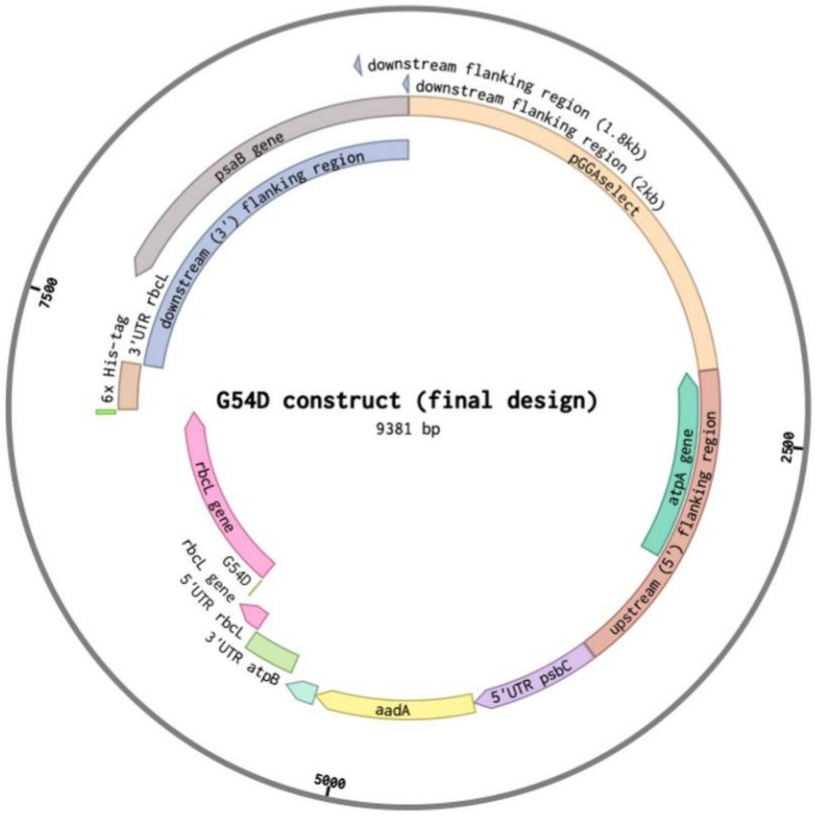
B
downstream flanking region (1.8kb)
downstream flanking region (2kb)
pGGAselect
psaB gene
downstream (3') flanking region
3'UTR rbcL
6x His-tag
G54D construct (final design)
9381 bp
rbcL gene
rbcL gene G54D
5'UTR rbcL
3'UTR atpB
aadA
5'UTR psbC
upstream (5') flanking region
atpA gene
7500
2500
5000

Supplementary Figure 8. Construct design of the *rbcL-G54D* mutant for future studies involving affinity purification and mass spectrometry. (A) The different components needed for the construct. Found on the left (insert 1) and right (insert 6) side of the linear construct are the 5' flanking and 3' flanking arms of the *rbcL* locus respectively, needed for homologous recombination. The *aadA* cassette is flanked by the 5'UTR and 3'UTR of other chloroplast genes (*psbC* and *atpB* respectively), and is required for antibiotic selection (inserts 2 and 3). Inserts 4 and 5 contain the gene of interest (*rbcL*), with the desired substitution and 6xHis-tag epitope for affinity purification and mass spectrometry. This figure was generated with Biorender. (B) Plasmid form (containing pGGAselect as the backbone) of the overall construct for the *rbcL-G54D* mutant. All required components described in (A) are found here. This figure was generated with Benchling.

Chlamydomonas strain CRC alias	Genotype	Rubisco/ Photoautotrophic	References
CC-4051	wild-type $4A^+$	+	(Kim *et al.*, 2005)
CC-125	wild-type 137c	+	(Pröschold *et al.*, 2005)
CC-3269	wild-type 2137	+	(Spreitzer & Mets, 1981)
CC-4691	*ΔrbcS-dim1*	-	(Dent *et al.*, 2005)
CC-4696	*ΔrbcL-MX3312*	-	(Satagopan & Spreitzer, 2004; Zhu *et al.*, 2010)
CC-4795	*rbcL-M42V*	+	(Du *et al.*, 2003)
CC-4796	*rbcL-C53A*	+	(Du *et al.*, 2003)
CC-4791	*rbcL-G54D*	-	(Spreitzer & Ogren, 1983; Spreitzer *et al.*, 1988, 1995)
CC-4719	*rbcL-C84S*	+	(Du & Spreitzer, 2000; Moreno *et al.*, 2008)
CC-4703	*rbcL-P89R*	+	(Larson *et al.*, 1997)
CC-4787	*rbcL-R217S*	-	(Thow *et al.*, 1994)
CC-4877	*rbcL-C247S*	+	(Knight *et al.*, 1990; Nozaki *et al.*, 2002)
CC-4720	*rbcL-C284S*	+	(Du & Spreitzer, 2000; Moreno *et al.*, 2008)
CC-4807	*rbcL-V331T*	+	(Chen & Spreitzer, 1989; Chen *et al.*, 1991)
CC-4831	*rbcL-C192S/Y226L*	-	(Esquível *et al.*, 2006)

Supplementary Table 1. Site-directed mutant strains of *Chlamydomonas reinhardtii* used throughout this thesis. All strains listed above are provided by the *Chlamydomonas* Resource Center (CRC), University of Minnesota.

Chlamydomonas strain name	Abbreviated name	*rbcL*	*rbcS*	Genotypes	Rubisco/ Photoautotrophic
ΔR T1.3	*ΔrbcL*	-	+	*ΔrbcL*	-
CAL B.C. 5.3	*ΔrbcS*	+	-	*ΔrbcS*	-
L2 mut #7xCal13 (L2 mut) T1.1	*rbcL-L2-mut*	+	+	*rbcL-E109A/R253A*	-
ARD #8 (L8 mut)	*rbcL-L8-mut*	+	+	*rbcL-A143W/R215A/D216A*	-
αAR (5'UTR *psaA:rbcL*)	5'UTR *psaA:rbcL*	+	+	*5'psaA:rbcL*	-
LStr #1	LS_{tr}	+	+	–––	-

Supplementary Table 2. Supramolecular state mutants of *Chlamydomonas reinhardtii* strains used throughout this thesis. All strains listed above are provided by Dr. Katia Wostrikoff from Sorbonne Université (Wietrzynski *et al.*, 2021).

Residues in WT RbcL of *Chlamydomonas*	Residues within 5 Å	Substituted Amino Acid	Residues within 5 Å	Stress Tolerance
M42	F40-P44, P50, C53, G54, V57, I87, N95-A99	M42V	F40-P44, C53, N95-A99	Significant to WT (High)
C53	M42, P44, V48-V57, A129, L130	C53A	M42, P44, V48-V57	Not significant to WT
G54	M42, P49-A58, C84, I87, A99, V101	G54D	Y24, Y25, M42, P49-A58, C84, Y85, D86, I87, A99, Y100, V101	Significant to WT (High – Dhaliwal, 2021)
C84	Y24-P27, G54, A55, A58, G82-I87, A99-A102	C84S	Y24-P27, G54, A55, A58, G82-I87, A99-A102	Not significant to WT (Low – Dhaliwal, 2021)
P89	I87-P91, Q96-I98	P89R	I87-P91, N95, Q96-I98	Not significant to WT (Low)
R217	A182, Y185, D202, V206-S208, M212-A222, L240, N241	R217S	A182, Y185, D202, M212-A222, L240	Not significant to WT (Low)
C192/Y226	C172, I174, A188-L197, T200, V221-E231, L260-V262, T406-L407, N413-A414, A417 Neighbouring RbcS1: S56, R59, F60, Y67, D69	C192S/ Y226L	C172, I174, A188-L197, T200, V221-E231, T406-L407, N413-A414, A417 Neighbouring RbcS: S56, R59, Y67, D69 Other neighbouring RbcS: N54	Significant to WT (High)
C247	G245-K252, A276 Dimer RbcL: C247, T275, A276, S279	C247S	G245-K252 Dimer RbcL: C247, T275, S279	Significant to WT (High)
C284	P152, H153, I265, L280-L291	C284S	P152, H153, I265, L280-L291	Significant to WT (High)
V331	G329-G333, L335, G337-R339, T342, I393, F394 Dimer RbcL: K128	V331T	G329-G333, L335, G337-R339, T342, I393, F394 Dimer RbcL: K128	Not significant to WT (Low)

Δ*rbcS*	-	-	-	Significant (High)
Δ*rbcL*	-	-	-	Not significant (Low)
L2-mut (E109/R253)	L107-S112, N115, Y144, N207, S208, W214, F218, N241, A242, A244, E249-A257 Dimer RbcL: E109, N207-Q209, T243-G245, R253	L2-mut (E109A/ R253A)	L107-S112, N115, Y144, W214, F218, N241, A242, E249-A257 Dimer RbcL: N207-Q209	Not significant (Low)
L8-mut (A143/R215/ D216)	T34, I105, P141-T147, A182, R213-F220, SMC256 (S-methylcysteine), Adjacent RbcL subunit: P152, H153, V157, K161, K258, R285-G288 Neighbouring RbcS: V63, C65 Second adjacent RbcL subunit: P142, A143, K146	L8-mut (A143W/ R215A/ D216A)	D33-T34, I105, P141-T147, V157, K161, A182, R213-F220, R285, D367, SMC369 (S-methylcysteine)	Significant (High)

Supplementary Table 3. Affected residues within 5 Å of the site-directed amino acid substitutions in RbcL seen in this thesis. Each mutant was analyzed in PyMol's Schrödinger-LLC program. The amino acid residue at each position was substituted for the one present in the mutants above. Stress tolerances are also indicated here.